Elastic Structure Preserving (ESP) Control for Compliantly Actuated Robots

Manuel Keppler, Dominic Lakatos, Christian Ott and Alin Albu-Schäffer

***Abstract*—Physical compliance can be considered one of the key technical properties a robot should exhibit to increase its mechanical robustness. In addition, the accompanying temporal energy storing capabilities enable explosive and energy efficient cyclic motions. But these advantages come at a price, as compliance introduces unwanted intrinsic oscillatory dynamics, underactuation, and reduces the natural frequency of the plant. These aspects make control of the link configuration variables a challenging task. This work presents two novel control methods for implementing link-side motion tracking capabilities and injecting a desired damping characteristic to suppress link vibrations along the reference trajectory for compliantly actuated robots with nonlinear elastic characteristics. We prove their uniform global asymptotic stability by invoking a theorem by Matrosov. Both approaches, namely ESP and ESP+, have in common that they preserve the link-side inertial properties and the elastic structure of the original plant dynamics, hence the name Elastic Structure Preserving control. Apart from that, ESP control focuses on preserving the inertial properties of motor dynamics. While ESP+ control aims at minimizing the dynamic shaping on the motor side. The performance of the feedback control laws have been evaluated on the variable stiffness robot arm DLR Hand Arm System, where the stiffness in each of its joints is highly nonlinear. To the best of our knowledge, this is the first experimentally validated tracking controller for compliantly actuated, multi-joint robots with nonlinear elastic elements.**

***Index Terms*—Tracking Control, Damping Control, Passivity-Based Control, Variable Stiffness Joints, Compliant Robots.**

I. Introduction

In order to increase the mechanical robustness against impacts and unknown contact forces, robot design recently evolved from rigid towards compliant actuators. While mechanical compliance provides many benefits it also comes at a price; the plant dynamics is under-actuated as the number of dimensions of the configuration space is twice the number of dimensions of the control input space. Moreover, to improve energy storing capabilities and efficiency in general, compliant actuators are often designed such that damping and friction in parallel to the spring is negligible. These intrinsic oscillatory dynamics can be exploited, for example for cyclic tasks like locomotion, hammering or drumming. For positioning tasks, however, these unwanted dynamics need to be handled in a proper manner to achieve positioning performances that come close to that of rigid manipulators. In addition, many variable stiffness robots feature highly nonlinear elasticity, see e.g Fig. 1(b). This is what makes control of the link configuration variables a challenging task.

The authors are with the Institute of Robotics and Mechatronics, German Aerospace Center (DLR), 82234 Oberpfaffenhofen, Germany,
e-mail: manuel.keppler@dlr.de,
see http://www.dlr.de/rmc/rm/en/staff/manuel.keppler.

Alin Albu-Schäffer is also with Technical University Munich, Chair of Sensor Based Robots and Intelligent Assistance Systems, Department of Informatics, D-85748 Garching, Germany.

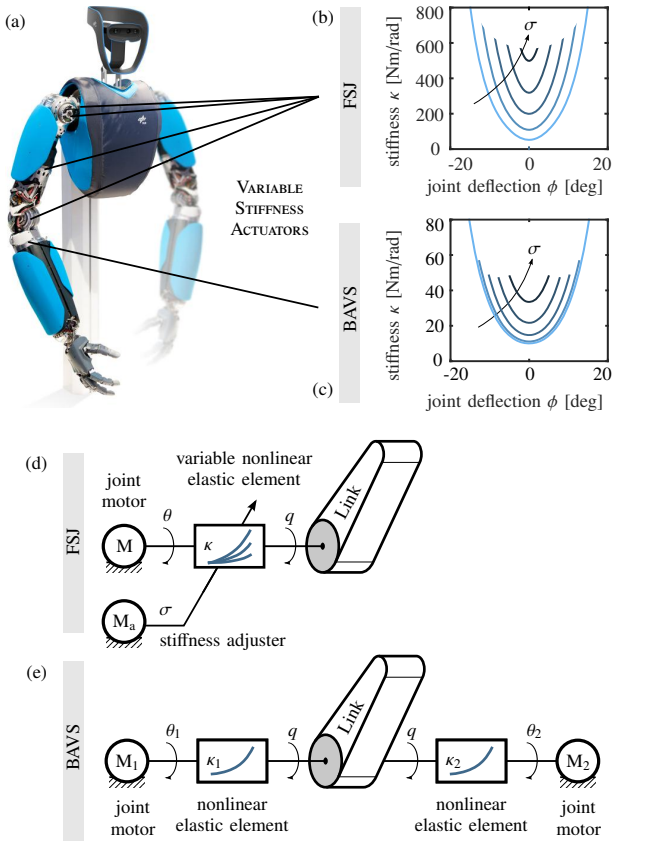

Fig. 1. DLR Hand Arms System [1]. (b) The first four arm joints, namely the elbow and the three shoulder joints, are implemented by Floating Spring Joints (FSJ) [2]. Joint stiffness characteristics for various stiffness adjuster positions $\sigma = [\,0, 2.5, 5.0, 7.5, 10\,]$ deg are shown. (c) Under arm rotation is realized by a Bidirectional Antagonistic Variable Stiffness (BAVS) joint [3]. Joint stiffness characteristics for different levels of co-contraction of the springs $\sigma = [\,0, 2.5, 5.0, 7.5, 10\,]$ deg are shown. (d-e) Simplified working schemes of the FSJ and BAVS joint are shown, respectively.

Regulation controllers for the link configuration variables of flexible joint robots (FJR) have been proposed in [4], [5], [6], [7] and a generalization to the case of nonlinear joint elasticities (often appearing in variable stiffness actuators (VSA) [8]) has been proposed in [9]. The above controllers consider only feedback of control-input-collocated variables. Therefore, the damping performance of these approaches is lower compared to the regulation controllers reported in [10], [11], [12] which feedback also control input non-collocated variables. While [10] provides a comprehensive stability analysis for constant

controller gains, the closed-loop dynamics of [11] and [12] are not accompanied by a rigorous stability proof.

Tracking controllers for the link configuration variables of robots with elastic transmissions are reported in the pioneering works [13], [14], [15]. Further solutions to the tracking problem are based on cascaded structures [16], integrator backstepping [17], [18, Chap. 6.2], extensions of the well known controller by Slotine and Li [19] to the flexible joint case [20], feedback linearization [13], [21], [22], and integral manifold control [13]. All of the tracking controllers above, [13]-[21], are formulated for linear elasticities with one exception: the method of [22] also applies to robots with nonlinear elasticities. Most of the tracking controllers above have been verified only in computer simulations.

Our primary objective is to develop an effective control approach that simultaneously achieves motion tracking and assignable damping for the link configuration variables of compliantly actuated robots, with nonlinear elastic transmissions, that is theoretically well founded (proof of global, uniform, asymptotic stability), practically feasible and achieves impressive performance (validation by experiments on a multi-VSA robot). This article presents a control concept — called *Elastic Structure Preserving* (ESP) control — that satisfies these goals. The development of the underlying idea was strongly driven by practical experience. Years of hands-on experience on the Hand Arm System indicated that approaches that change the elastic behavior and the dynamics in general, respectively, to a 'high' degree — albeit being theoretically sound — are prone to fail in practice. The main reasons for this are limited robustness to unmodeled dynamics, parameter uncertainties, actuator bandwidth and amplitude limitations. This insight led to the idea of designing a control approach that relies on the fundamental concept of changing the original dynamics only to a minimal extent and in particular of preserving the (nonlinear) elastic structure; hence the name ESP control. And, indeed, we can show on the basis of a theoretical analysis for a single joint, that our approach changes the plant dynamics significantly less than feedback linearization-based full state feedback (FSF) control and hence, suffers less from the aforementioned issues.

Interestingly, the dynamics gravity cancellation control law for flexible robots proposed in [23] is contained in our approach.

The ESP control concept was first introduced in our previous work [24]. It relies on adding only damping and feedforward terms to the dynamics of the link variables while neither changing the plant inertia properties nor the structure of the nonlinear springs. By introducing new coordinates that reflect these damping and feedforward terms and a corresponding coordinate transformation of the motor dynamics, we achieved, through means of feedback control, a closed-dynamics which structurally equals the dynamics of the original coordinates, but with the added link damping. To achieve, in addition, the desired tracking (and disturbance rejection) behavior of the link coordinates we implement pure PD regulation control in the new motor coordinates.

The work [25], further extends the concept of "minimalistic" feedback control to solve the damping and tracking problem for the link configuration variables of compliantly actuated robots. This is done by avoiding the scaling of the motor inertia to constant values in the new coordinates which is a non-passive control action for itself.[1] We refer to this approach as ESP+.

This article introduces the underlying concept in greater detail (see Sec. III), compares the ESP and ESP+ control approaches, and extends the stability analysis. In our previous works [24], [25] we have shown global stability of the corresponding closed-loop dynamics. The main result of this work extends these statements to global, uniform asymptotic stability, which is presented in Sec. VI. On the basis of the ESP and ESP+ controller formulation introduced in this paper, we show that in the limiting case of rigid actuation (i. e., the stiffness parameters approach infinite values) the classical PD+ controller [27] results for both approaches. In this paper we show that in contrast to many state of the art FJR controllers, no high-gain design results in this limiting case (cf. [28, chapt. 4.1]). Moreover, we conceptionally proove that our approach performs less dynamics shaping than feedback linearization-based FSF control.

The paper is structured as follows: the underlying idea is presented in Sec. III and the problem is formulated in Sec. II. Sec. IV proposes the ESP and ESP+ controller designs and provides a short discussion. Sec. V proves passivity of the closed-loop dynamics. Sec. VI contains an extensive stability analysis. Finally, experimental validation is provided in Sec. VII and Sec. VIII briefly concludes the work.

A. Notation and Terminology

Throughout the text, when talking about the boundedness of vectors and matrices we refer to it in the sense of bounded Euclidean norms, $\|.\|$, and bounded eigenvalues, respectively. Let Ω be a domain and I a set. Consider a quadratic matrix $\boldsymbol{A}(t,\boldsymbol{x})$, defined for all $(t,\boldsymbol{x}) \in I \times \Omega$, then $\underline{\lambda}(\boldsymbol{A})$ and $\bar{\lambda}(\boldsymbol{A})$ denote its minimum and maximum eigenvalue, respectively, i.e.

$$\underline{\lambda}(\boldsymbol{A}(t,\boldsymbol{x})) := \inf_{t\in I,\boldsymbol{x}\in\Omega} \lambda(\boldsymbol{A}(t,\boldsymbol{x})),$$
$$\bar{\lambda}(\boldsymbol{A}(t,\boldsymbol{x})) := \sup_{t\in I,\boldsymbol{x}\in\Omega} \lambda(\boldsymbol{A}(t,\boldsymbol{x})).$$

Analogously, $\underline{\sigma}(\boldsymbol{A})$ and $\bar{\sigma}(\boldsymbol{A})$ denote the minimum and maximum singular value of $\boldsymbol{A}$, respectively. C^k denotes the space of k-times continuously differentiable functions.

II. Problem Statement

Throughout this paper, we consider a simplified model of a n-link robot with compliant joints which is based on the model proposed by [13] and assumes that the angular part of the kinetic energy of each rotor is due only to its own rotation, and is given by

$$\boldsymbol{M}(\boldsymbol{q})\ddot{\boldsymbol{q}} + \boldsymbol{C}(\boldsymbol{q},\dot{\boldsymbol{q}})\dot{\boldsymbol{q}} = -\boldsymbol{g}(\boldsymbol{q}) + \boldsymbol{\psi}(\boldsymbol{\theta}-\boldsymbol{q}) + \boldsymbol{\tau}_{ext} \quad (1)$$
$$\boldsymbol{B}\ddot{\boldsymbol{\theta}} + \boldsymbol{\psi}(\boldsymbol{\theta}-\boldsymbol{q}) = \boldsymbol{u}. \quad (2)$$

[1] The concept of inertia scaling was first introduced in [26].

Herein, $\boldsymbol{q} \in \mathbb{R}^n$ and $\boldsymbol{\theta} \in \mathbb{R}^n$ represent the link angles and motor angles, respectively. $\boldsymbol{M} \in \mathbb{R}^{n\times n}$ is the inertia matrix of the rigid links, $\boldsymbol{B} \in \mathbb{R}^{n\times n}$ is the diagonal matrix of the actuator inertias reflected through the respective gearboxes[2]. They have the following properties:

Property 1. *The mass matrices $\boldsymbol{M}(\boldsymbol{q})$ and $\boldsymbol{B}$ are symmetric, positive definite.*

Property 2. *The singular values of $\boldsymbol{M}(\boldsymbol{q})$ and $\boldsymbol{B}$ are bounded above and bounded below away from zero, thus both $\boldsymbol{M}^{-1}(\boldsymbol{q})$ and $\boldsymbol{B}^{-1}$ exist and are bounded.*

These conditions are fulfilled for all pure rotational and pure prismatic joint robots and in some special cases for robots that feature a mix of rotational and prismatic joints, see [29] for an in-depth discussion. We denote the vector of Coriolis and centrifugal forces by $\boldsymbol{C}(\boldsymbol{q},\dot{\boldsymbol{q}})\dot{\boldsymbol{q}}$. Vector $\boldsymbol{g}(\boldsymbol{q})$ represents the gravitational forces. As suggested by [20], we define $\boldsymbol{C}(\boldsymbol{q},\dot{\boldsymbol{q}})$ via the Christoffel symbols, such that model (1)-(2) features the following properties:

Property 3. *Since $\boldsymbol{C}(\boldsymbol{q},\dot{\boldsymbol{q}})$ is bounded in $\boldsymbol{q}$ and linear in $\dot{\boldsymbol{q}}$, $\boldsymbol{C}$ is bounded for bounded $\dot{\boldsymbol{q}}$. The matrix $\dot{\boldsymbol{M}}(\boldsymbol{q}) - 2\boldsymbol{C}(\boldsymbol{q},\dot{\boldsymbol{q}})$ is skew symmetric for all $(\boldsymbol{q},\dot{\boldsymbol{q}}) \in \mathbb{R}^n \times \mathbb{R}^n$.*

The dynamics (1)–(2) represents an under-actuated mechanical system in which only the generalized motor coordinates $\boldsymbol{\theta}$ can be directly actuated via the generalized motor forces $\boldsymbol{u} \in \mathbb{R}^n$, which will serve as the control input. The link coordinates $\boldsymbol{q}$ can only be indirectly actuated via the generalized elastic forces $\boldsymbol{\psi}$ which are derived from the spring potential function U_s. This form of under-actuation is the major challenge in the control of the states $\boldsymbol{q},\dot{\boldsymbol{q}}$. We assume the following properties for U_s:

Assumption 1. *The elastic potential function $U_s(\boldsymbol{\phi}) \in C^4$ is strongly convex and positive definite for all $\boldsymbol{\phi} \in \mathbb{R}^n$, i.e. $U_s(\boldsymbol{\phi}) = 0 \implies \boldsymbol{\phi} = \boldsymbol{0}$.*[3]

Assumption 2. *The generalized elastic forces $\boldsymbol{\psi}(\boldsymbol{\phi})$ can be derived from the spring potential function U_s*

$$\boldsymbol{\psi}(\boldsymbol{\theta}-\boldsymbol{q}) \coloneqq \left(\frac{\partial U_s(\boldsymbol{\phi})}{\partial \boldsymbol{\phi}}\right)\Bigg|_{\boldsymbol{\phi}=\boldsymbol{\theta}-\boldsymbol{q}} \in \mathbb{R}^n. \tag{3}$$

Strong convexity of U_s ensures that a constant $c > 0$ exists such that

$$\inf_{\boldsymbol{\phi}\in\mathbb{R}^n} \underline{\lambda}\left(\frac{\partial \boldsymbol{\psi}(\boldsymbol{\phi})}{\partial \boldsymbol{\phi}}\right) > c, \quad \forall \boldsymbol{\phi} \in \mathbb{R}^n. \tag{4}$$

Loosely speaking, $\boldsymbol{\psi}$ is strictly monotonic in its argument. As the Jacobian determinant of $\boldsymbol{\psi}$ is nonzero due to (4), the inverse function theorem guarantees that $\boldsymbol{\psi}$ is a global diffeomorphism. The local stiffness, i.e. the Hessian of the spring potential U_s, is denoted as follows

$$\boldsymbol{\kappa}(\boldsymbol{\phi}_0) \coloneqq \left(\frac{\partial^2 U_s(\boldsymbol{\phi})}{\partial \boldsymbol{\phi}^2}\right)\Bigg|_{\boldsymbol{\phi}=\boldsymbol{\phi}_0} = \frac{\partial \boldsymbol{\psi}(\boldsymbol{\phi})}{\partial \boldsymbol{\phi}}\Bigg|_{\boldsymbol{\phi}=\boldsymbol{\phi}_0} \in \mathbb{R}^{n\times n}. \tag{5}$$

$\boldsymbol{\tau}_{ext}$ represents the generalized external forces which are exhibited by the manipulators environment.

In this paper we address the problem of finding a control concept that achieves the following characteristics. In absence of external disturbances, it achieves uniform global asymptotic link-side motion tracking behavior. Further, it adds a velocity proportional damping term $\boldsymbol{D}\dot{\tilde{\boldsymbol{q}}}$ on the link side.[4] For the tracking case, this damping acts on the velocity tracking error $\dot{\tilde{\boldsymbol{q}}}$. While achieving this, the intrinsic compliance and the inertia properties of the system shall be preserved.

Loosely speaking, we aim at deriving a control concept that enables compliant robots to interact via their environment with their intrinsic compliance but in a damped fashion; see videos of the experiments in Sec. VII.

III. Design Idea

This section presents the basic design idea that underlies the proposed control laws. We consider a single robotic joint featuring a linear-elastic transmission as depicted in 2(a). In order to keep the presentation of the design idea simple we consider the simplified case of a linear-elastic element in this section only. The general case of nonlinear elastic elements is treated in Sec. IV. The corresponding dynamic model is given by

$$M\ddot{q} = K(\theta - q) \tag{6}$$

$$B\ddot{\theta} + K(\theta - q) = u. \tag{7}$$

The control input u is a generalized force acting on the motor inertia B which drives the link inertia M via an intermediate spring with stiffness K. The generalized spring force is given by $K(\theta - q)$, where θ and q are the motor and link coordinates, respectively.

First, we consider the gravity-free, link-side regulation case. Thereafter, we extend the concept to the link-side tracking case.

A. Link-Side Damping and link-side Regulation

We consider the problem of finding a feedback control u that adds a desired link-side damping behavior and regulates the link position q to a desired link position q_d, while preserving the intrinsic stiffness K and inertial properties of the plant.

With this in mind, we consider a reference joint that features link-side, velocity-proportional damping, but otherwise equal inertial and elastic properties; as shown in Fig. 3. The according dynamics model is given by

$$M\ddot{\rho} = K(\eta - \rho) - D\dot{\rho} \tag{8}$$

$$B\ddot{\eta} + K(\eta - \rho) = \bar{u}, \tag{9}$$

[2]More precisely, the motor inertias about their principal axis of rotation are multiplied by the square of the respective gear ratios, see [13] for further details.

[3]The strong convexity is no limiting condition from a practical point of view, as a lower bound for the joint stiffness is necessary such that the robot does not collapse under it's gravitational weight and thus becomes uncontrollable.

[4]We are convinced, due to the reasons mentioned in the introduction, that being able to add link-side damping via control is essential in order to make compliantly actuated robots practically feasible.

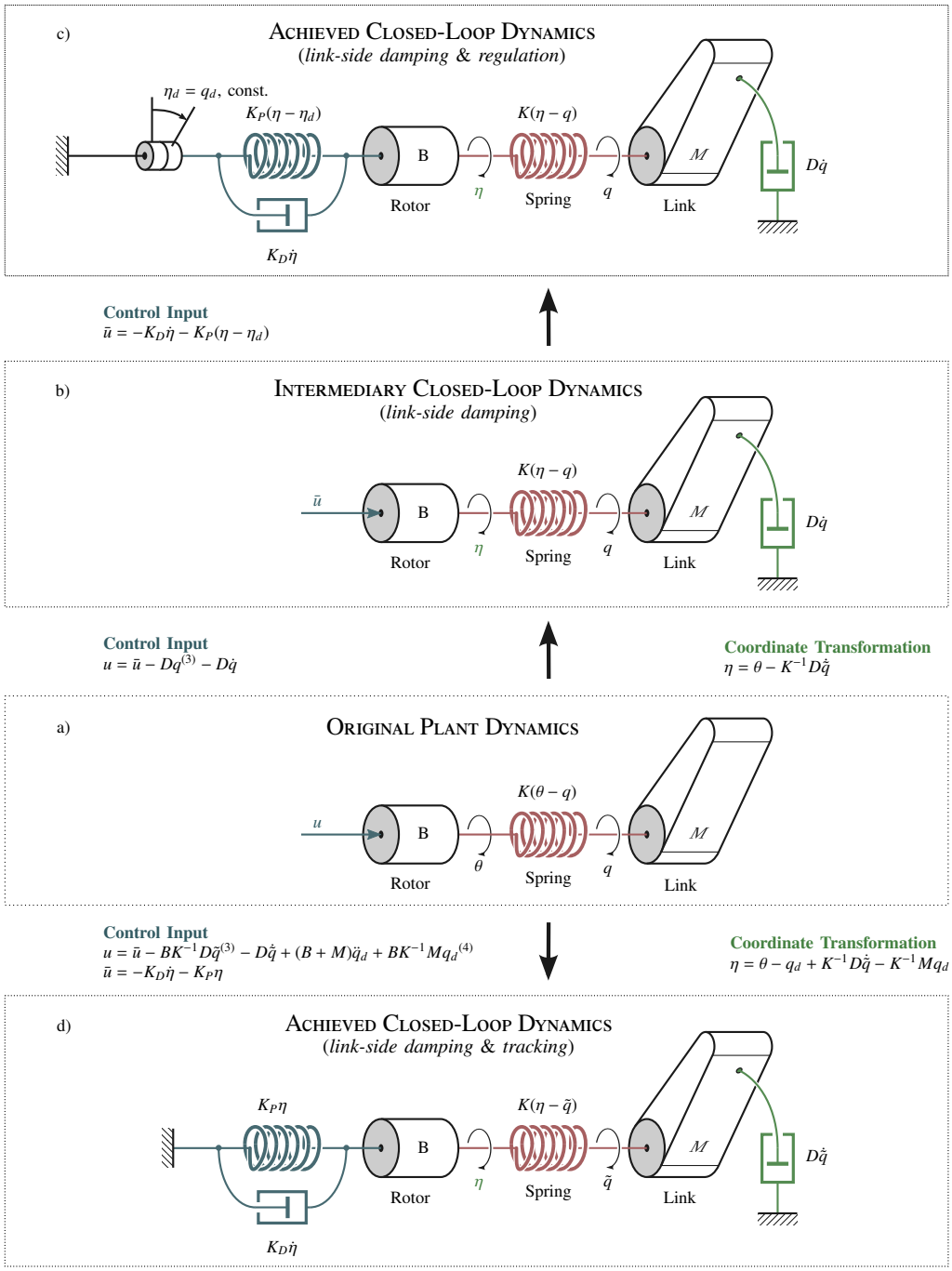

$\theta \ldots$ motor coord. $q \ldots$ link coord. $q_d \ldots$ des. link pos. $\tilde{q} := q - q_d(t) \ldots$ tracking error $\eta \ldots$ new motor coord. $\eta_d := q_d \ldots$ des. new motor coord.

Fig. 2. (a) Visualization of the Elastic Structure Conserving (ESC) control concept for a single joint with constant stiffness K and control input u. The steps for the regulation approach (Fig. 2.(b–c)) can be interpreted as follows. First, we inject damping to the link side. To this end, we introduce new motor coordinates and an intermediary control law, such that the resulting intermediary system, written in the new coordinates, structurally equals the original dynamics. Second, we shape the potential energy of the rotor of the intermediary system by introducing a spring with stiffness K_P. An additional velocity-proportional damper is introduced to modify the convergence behavior of the motor. The link equilibrium point of the resulting system is unique and coincidences with the desired link position if $\eta_d = q_d$. For the tracking case we proceed in an analog way. With difference being, that some pseudo feed-forward terms are added to the coordinate transformation and the intermediary control input. The resulting error dynamics are represented graphically in Fig. 2(d). As desired, the corresponding unique equilibrium lies at the origin, i.e. $\eta = \tilde{q} = 0$. Note, the systems elastic structure is being conserved in all cases, Fig. 2(b–d), hence, the name ESP control. For both, the regulation and tracking case, the stiffness of the real physical spring acts as proportional gain to drive the link position.

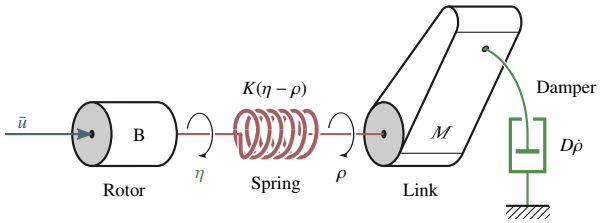

Fig. 3. Joint with damped link.

where η and ρ are the motor and link coordinates, respectively. The damping behavior is characterized by the positive damping gain D.

If we manage our original system to behave equivalently to this reference system, we would have accomplished our first design goal. Thus, we ask the question: can we find a control input u for our original joint (6)–(7), such that it behaves like the damped joint (8)–(9) with control input $\bar{u}$? In particular, we want the link of the original system to behave identical to the damped link of the reference system. As such, we impose equality of the link coordinates

$$q(t) \stackrel{!}{=} \rho(t), \qquad \forall t \in [t_0, \infty). \tag{10}$$

We assume that such control input u exists and proceed. First, we force equivalence of the link dynamics (6) and (8). To this end, under consideration of eq. (10), we equate the RHS of (6) and (8). This yields the following coordinate transformation

$$\theta = \eta - K^{-1} D\dot{q}, \tag{11}$$

Next, we aim to achieve equivalence of the motor dynamics (7) and (9). For this purpose, we introduce the following intermediary control law

$$u = \bar{u} - BK^{-1} Dq^{(3)} - D\dot{q}. \tag{12}$$

System (6)–(7) under control law (12) and under consideration of the coordinate transformation (11) (substitution of θ and $\ddot{\theta}$) gives the following intermediary closed-loop dynamics

$$M\ddot{q} = K(\eta - q) - D\dot{q} \tag{13}$$

$$B\ddot{\eta} + K(\eta - q) = \bar{u}. \tag{14}$$

Figure 2(b) shows the corresponding graphical representation of the dynamics (13)–(14). With (10) in mind, we have confirmed our assumption.

Up to this point, we have achieved that system (6)–(7), under the action of the intermediary control law (12) — cf. eq. (13)–(14) — is equivalent to the reference system (8)–(9). As such, for all time $t \in [t_0, \infty)$ and for any control input $\bar{u}(t)$, the link position of the original system (6)–(7) under control action (12), and that of the damped reference system (8)–(9) evolve equivalently; under the assumption that both systems are initialized equally, i.e. $q^{(i)}(t_0) = \rho^{(i)}(t_0), \ \forall i \in \{0, 1, 2, 3\}$. This completes the proof of our initial assumption and the first part of our control design.

Remark 1. Thus far, u is composed of terms that are just sufficient to achieve equivalence of systems (6)–(7) and (8)–(9). In that regard, we have modified the dynamics to a minimal extend.

So far $\bar{u}$ is still open to further control design and allows us to fulfill the second design goal of adding link-side regulation behavior. For any command $\bar{u}$, the intermediary closed-loop dynamics (13)–(14) and the damped reference system (8)–(9) evolve exactly the same. With this in mind, a natural and simple way to add link-side regulation behavior is motor PD control in the new motor coordinate

$$\bar{u} = -K_D\dot{\eta} - K_P(\eta - \eta_d), \tag{15}$$

with $\eta_d := q_d$, constant. Note, that the resulting closed-loop dynamics

$$M\ddot{q} = K(\eta - q) - D\dot{q} \tag{16}$$

$$B\ddot{\eta} + K(\eta - q) = -K_D\dot{\eta} - K_P(\eta - \eta_d) \tag{17}$$

can still be interpreted as a multi-spring-damper system. A graphical representation is shown in Fig. 2(c). The proportional gain K_P [indicated by the blue spring in Fig. 2(c)] drives the system to its new equilibrium state — the desired link regulation behavior $q \to q_d$ for $t \to \infty$, is achieved. Formally, global, asymptotic stability of the unique equilibrium state $\eta = \theta = q_d, q = q_d$ can be shown by invoking La'Salles theorem [30].[5]

Remark 2. Now, the second fundamental design idea becomes clear. We add simple motor PD control to achieve regulation and later tracking behavior. As such, the link and motor remain connected via the original elastic transmission (highlighted in red in Fig. 2(a–c.). In other words, we use the stiffness of the real physical spring as the proportional controller gain to drive the link position.

B. ESP Control vs. Feedback Linearization

In this section we perform a gain analysis where we compare ESP control in full state feedback (FSF) form with feedback linearization-based FSF control. We perform this analysis exemplary on the basis of the DLR Hand Arm System. Its inertia is highly configuration dependent, it varies significantly throughout its workspace. Let us consider the first five joints of the right arm. The first joint faces an inertia M that depends on the configuration of the other joints as visualized in Fig. 4. More specifically, M ranges from $M_{min} = 0.01\ \mathrm{kg\,m^2}$ (left pose) to $M_{max} = 1.1\ \mathrm{kg\,m^2}$ (right pose). Similarly, the stiffness K of the first joint (cf. Fig. 1) varies between $K_{min} = 40\ \mathrm{Nm\,rad^{-1}}$ and $K_{max} = 900\ \mathrm{Nm\ rad^{-1}}$, depending on the stiffness setting σ and the external load.

For our analysis, we consider again a single robotic joint as shown in Fig. 2(a), but this time we assume that the link inertia and joint stiffness can take a range of values, i.e. $M \in [M_{min}, M_{max}]$ and $K \in [K_{min}, K_{max}]$, as it would be the case for the first axis of the DLR Hand Arm System.

We can write the ESP Control approach for the gravity-free regulation case in full state feedback (FSF) form with state vector $\boldsymbol{x} = [\ q\ \dot{q}\ \ddot{q}\ q^{(3)}\ ]$. To this end, we solve (6) for θ and

[5]One feasible, physically-motivated Lyapunov function candidate is $V = 1/2\left(M\dot{q}^2 + B\dot{\eta}^2 + K(\eta - q)^2 + K_P(\eta - \eta_d)^2\right)$; its time derivative along the solutions of (16)–(17) is $\dot{V} = -D\dot{q}^2 - K_D\dot{\eta}^2 \leq 0$.

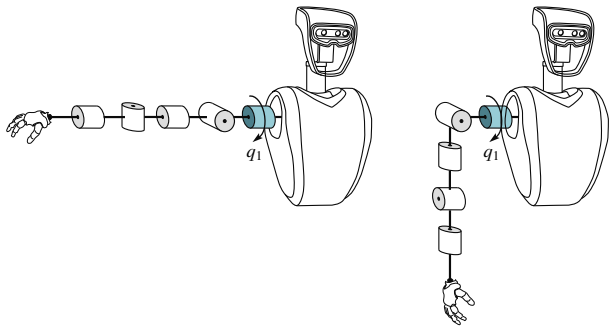

Fig. 4. The minimum and maximum inertia configurations with respect to the first joint of the DLR Hand Arm System are shown.

substitute that relation in (11) to yield a relation between η and q, and its time-derivatives, only

$$\eta = K^{-1}M\ddot{q} + K^{-1}D\dot{q} + q. \tag{18}$$

Substituting this relation in (15) allows us to re-write controller (12) in full state feedback form. Without loss of generality we assume $\eta_d = q_d = 0$ and choose the damping coefficients as follows[6]: $D = 2\xi_1\sqrt{MK}$ and $K_D = 2\xi_2\sqrt{BK}$, with $\xi_1 = \xi_2 = 0.7$, this results in

$$u = -\boldsymbol{k}^d\boldsymbol{x}, \tag{19}$$

where $\boldsymbol{k}_d$ is the gain matrix with the following components

$$k_1^d = K_P \tag{20}$$

$$k_2^d = 2(1 + \frac{K_P}{K})\xi_1\sqrt{MK} + 2\xi_2\sqrt{BK} \tag{21}$$

$$k_3^d = 2\frac{D}{K}\xi_1\sqrt{MK} + \frac{K_P}{K}M \tag{22}$$

$$k_4^d = 2\frac{B}{K}\xi\sqrt{MK} + 2\frac{M}{K}\xi_2\sqrt{BK}. \tag{23}$$

We now derive a feedback linearization-based FSF controller. By solving (7) with respect to $\ddot{\theta}$ and substituting it in the second time derivative of (6), we can re-write system (7)–(6) in the form of the following 4-th order differential equation

$$q^{(4)} = \frac{K}{BM}u - K\left(\frac{1}{B} + \frac{1}{M}\right)\ddot{q}. \tag{24}$$

In order to input-state linearize the system, we choose the control input u as[7]

$$u^f = \frac{BM}{K}v + (B + M)\ddot{q}, \tag{25}$$

resulting in the following linear controllability canonical form

$$\dot{\boldsymbol{x}} = \begin{bmatrix} \boldsymbol{0}_{3\times1} & \boldsymbol{I}_{3\times3} \\ 0 & \boldsymbol{0}_{1\times3} \end{bmatrix}\boldsymbol{x} + \begin{bmatrix} \boldsymbol{0}_{3\times1} \\ 1 \end{bmatrix}v, \tag{26}$$

where $\boldsymbol{x}$ is the new state vector and v is the new control input. Again, we choose full state feedback control

$$v = -\boldsymbol{k}\boldsymbol{x}, \tag{27}$$

[6]See Sec. VII-A for details about the damping design.

[7]To assure controllability we have to assume $K > 0$ and $BM < \infty$.

where $\boldsymbol{k} = [\,k_1\,k_2\,k_3\,k_4\,]$. Substituting (27) in (25) gives the final control law

$$u_f = -\boldsymbol{k}^f\boldsymbol{x} = -\frac{BM}{K}\begin{bmatrix} k_1 & k_2 & k_3 - \frac{K}{BM}(B+M) & k_4 \end{bmatrix}\boldsymbol{x}, \tag{28}$$

where $\boldsymbol{k}^f = [\,k_1^f\,k_2^f\,k_3^f\,k_4^f\,]$. We now choose $k_1, \ldots, k_4$ such that k^d equals k_f for the case that the link inertia and joint stiffness assume the following reference values: $M_{ref} = 0.1$ kg m^2 and $K_{ref} = 200$ Nm/rad, respectively, i.e. $k_1 = K_P\frac{K_{ref}}{BM_{ref}}$ etc. The reference values were chosen such that they are located magnitude-wise in the center of their respective range. As such, for the reference case M_{ref} and K_{ref}, both controllers are identical; hence they achieve the same closed-loop dynamics. Starting from this reference point we are now interested in how the gains $\boldsymbol{k}^d$ and $\boldsymbol{k}^f$ change if the link inertia and joint stiffness deviate from their respective reference values. Figure 5 and 6 show the results of this analysis. The white sphere marks the reference case, where M and K assume their reference values and $\boldsymbol{k}^d$ and $\boldsymbol{k}^f$ coincide.

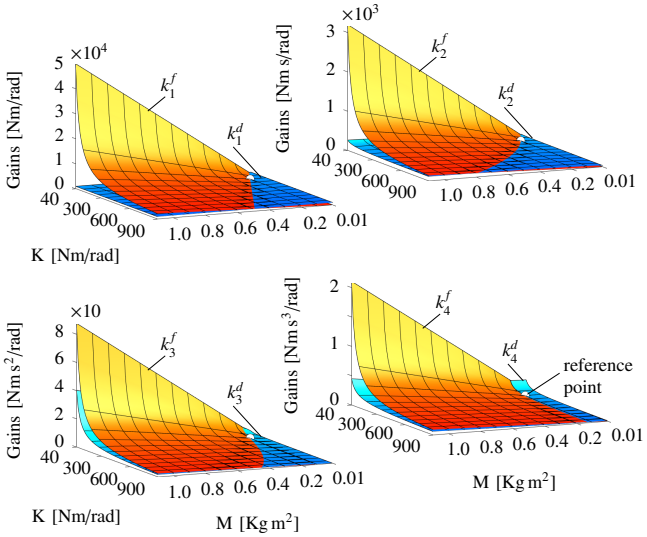

Fig. 5. $\boldsymbol{k}^d$ and $\boldsymbol{k}^f$ as a function of the link inertia M and joint stiffness K. Clearly, the feedback linearization gains $\boldsymbol{k}^f$ vary significantly stronger with changing inertia and stiffness values than the ESP gains $\boldsymbol{k}^d$.

Clearly, the elements of $\boldsymbol{k}^f$ vary significantly stronger than those of $\boldsymbol{k}^d$. This has several theoretical and practical implications. Compared to feedback linearization, ESP is less susceptible to input saturation and shows less sensor noise amplification. Moreover, from experience we know that gains on q and $\dot{q}$ as high as 5×10^4 N m/rad and 3×10^3 N m/rad, respectively, are not realizable on the Hand Arm System. It is also clear that uncertainties in K and M have a much larger impact on the gains for feedback linearization than for ESP control. These findings allow the conclusion that ESP control shapes the plant dynamics significantly less than feedback linearization.

C. Link-Side Damping and Link-Side Tracking

We now adopt the design ideas introduced for the regulation case III-A, to find a control law, that simultaneously achieves link-side damping and asymptotic, link-side tracking, for the system (6)–(7).

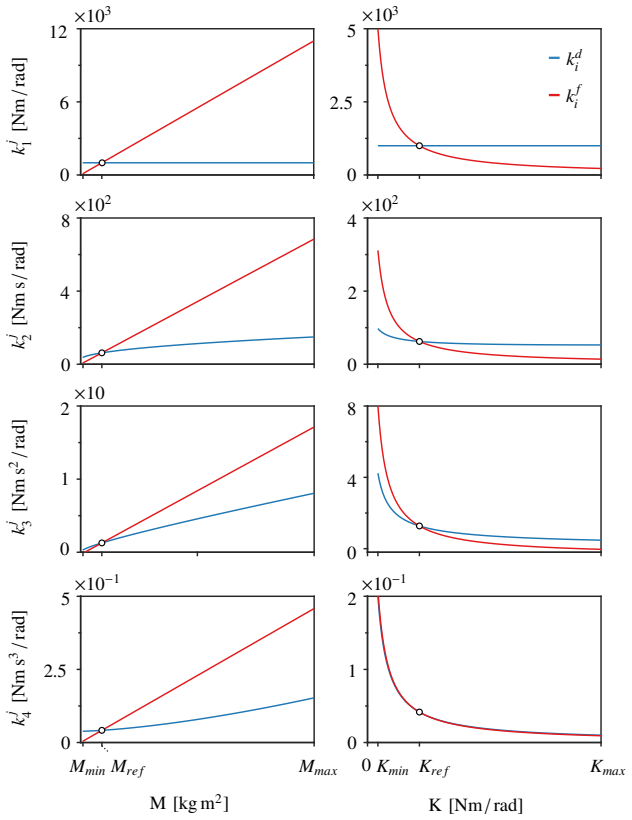

Fig. 6. $\boldsymbol{k}^d$ and $\boldsymbol{k}^f$ as a function of the link inertia M and joint stiffness K, respectively. The plots show planar, vertical cuts of Fig. 5 that run parallel to the M and K axis, respectively, and intersect the reference point

Let $q_d(t) \in \mathbb{C}^4$ be the desired nominal motion trajectory. Instead of studying the deviation of $q(t)$ from $q_d(t)$ for the controlled system, we transform the stability problem into an equivalent one that studies the temporal variation of the motion error $\tilde{q}(t) := q(t) - q_d(t)$. Thereby, we simplify the control problem to finding a control input that stabilizes the origin. Again we try to change the dynamics of the original system to a minimal extent. Therefore, we extend the link-dynamics solely by a damping term and pseudo[8] feed forward terms that ensure tracking performance. With that in mind, in the following, we derive a control input u for (6)–(7), such that the link behavior of the resulting compensated system equals

$$M\ddot{\tilde{q}} = K(\eta - \tilde{q}) - D\dot{\tilde{q}} \tag{29}$$

Compared to the regulation case, we choose a more straight forward approach[9] and start with the coordinate transformation right away. The link dynamics (6) and (29) are equivalent if and only if

$$K(\theta - q) = K(\eta - \tilde{q}) - D\dot{\tilde{q}} + M\ddot{q}_d. \tag{30}$$

[8]In fact, for the 1 DoF case with linear spring, $M\ddot{q}_d, D\dot{q}_d, Kq_d$ actually are feed forward terms, but this won't be the case for the general, multi-dof case with nonlinear transmissions, cf. (38).

[9]This way is superior for the general case described in Section IV as it helps to keep the equations more compact.

This time, the new motor coordinate η reflects the desired damping and tracking behavior. It can easily be verified that the system (6)–(7) under the intermediary control law

$$u = \bar{u} \underbrace{-BK^{-1}D\tilde{q}^{(3)} - D\dot{\tilde{q}}}_{\text{damping terms}} \underbrace{+BK^{-1}Mq_d{}^{(4)} + (B+M)\ddot{q}_d}_{\text{tracking terms}} \tag{31}$$

and under consideration of the coordinate transformation (30), results in the following intermediary, closed-loop dynamics

$$M\ddot{\tilde{q}} + D\dot{\tilde{q}} = K(\eta - \tilde{q}) \tag{32}$$

$$B\ddot{\eta} + K(\eta - \tilde{q}) = \bar{u}. \tag{33}$$

Thus, the problem is reduced to finding a control input $\bar{u}$ that drives η and therefore $\tilde{q}$ to the origin. Analogously to the regulation case, we choose a PD control in the new motor coordinates[10]

$$\bar{u} = -K_D\dot{\eta} - K_P\eta. \tag{34}$$

This leaves us with the following closed-loop dynamics

$$M\ddot{\tilde{q}} - K(\eta - \tilde{q}) + D\dot{\tilde{q}} = 0 \tag{35}$$

$$B\ddot{\eta} + K(\eta - \tilde{q}) = -K_D\dot{\eta} - K_P\eta. \tag{36}$$

Again the closed-loop dynamics can be represented by a multi-spring-damper system as visualized in Fig. 2(d). This provides us with an physically intuitive understanding of the closed-loop behavior.

D. Outlook

The remainder of the paper applies these basic ideas to general robotic systems

- with nonlinear elastic transmissions,
- with multiple degrees of freedom,
- that are subject to gravity.

In addition we extend the concept of minimizing the dynamic shaping from the link to the motor side, which is relevant for systems with nonlinear joint elasticities.

IV. Controller Design

This section extends the control concept presented in Sec. III to general robotic systems that are subject to gravity and feature multiple degrees of freedom and nonlinear elastic transmissions.

A. Desired Link-Side Dynamics

We extend the link-side dynamics solely by a damping term and pseudo feed forward terms that ensure tracking performance. With that in mind, in the following, we derive a control input $\boldsymbol{u}$ in (2), such that the link-side behavior of the resulting compensated system equals the following desired dynamics[11]

$$\boldsymbol{M}(t,\tilde{\boldsymbol{q}})\ddot{\tilde{\boldsymbol{q}}} + \boldsymbol{C}(t,\tilde{\boldsymbol{q}},\dot{\tilde{\boldsymbol{q}}})\dot{\tilde{\boldsymbol{q}}} = -\boldsymbol{D}\dot{\tilde{\boldsymbol{q}}} + \boldsymbol{\psi}(\boldsymbol{\eta} - \tilde{\boldsymbol{q}}) + \boldsymbol{\tau}_{ext}, \tag{37}$$

[10]Albeit the structure of the PD control laws (15) and (34) being the same, they differ due to the differing coordinate transformation.

[11]With better readability in mind and to emphasize the explicit time dependency of the closed-loop link dynamics, we use the short forms $\boldsymbol{M}(\tilde{\boldsymbol{q}},t) := \boldsymbol{M}(\boldsymbol{q}) = \boldsymbol{M}(\tilde{\boldsymbol{q}} + \boldsymbol{q}_d(t))$, $\boldsymbol{C}(\tilde{\boldsymbol{q}},\dot{\tilde{\boldsymbol{q}}},t) := \boldsymbol{C}(\boldsymbol{q},\dot{\boldsymbol{q}}) = \boldsymbol{C}(\tilde{\boldsymbol{q}} + \boldsymbol{q}_d(t), \dot{\tilde{\boldsymbol{q}}} + \dot{\boldsymbol{q}}_d(t))$ and $\boldsymbol{g}(\tilde{\boldsymbol{q}},t) := \boldsymbol{g}(\boldsymbol{q}) = \boldsymbol{g}(\tilde{\boldsymbol{q}} + \boldsymbol{q}_d(t))$.

where $\tilde{\boldsymbol{q}} := \boldsymbol{q} - \boldsymbol{q}_d(t) \in \mathbb{R}^n$ is the link-side tracking error. The desired trajectory has the following properties:

Assumption 3. *$\boldsymbol{q}_d(t) \in C^4$, with $\|\boldsymbol{q}_d\|, \|\dot{\boldsymbol{q}}_d\|, \ldots, \|\boldsymbol{q}_d^{(4)}\|$ being bounded.*

$\boldsymbol{\eta} \in \mathbb{R}^n$ are suitable motor coordinates, that reflect the desired link-dynamics. They will be introduced later.

The damping matrix $\boldsymbol{D}$ allows to realize a desired link-side damping behavior, such that $\dot{\tilde{\boldsymbol{q}}} \to \boldsymbol{0}$. $\boldsymbol{D}$ has to meet the following conditions:

Assumption 4. *The damping matrix $\boldsymbol{D} \in \mathbb{R}^{n\times n}$ is positive definite, lower and upper bounded. $\boldsymbol{D}$ might even be a C^2 function of $\boldsymbol{\eta}$, $\tilde{\boldsymbol{q}}$ and t. In this case, to satisfy the conditions of the implicit function theorem, such that $\boldsymbol{\eta}$ can be (locally) expressed as a function of the other coordinates, $\det\left(\frac{\partial \boldsymbol{n}}{\partial \boldsymbol{\eta}}(t, \boldsymbol{\eta}, \tilde{\boldsymbol{q}}, \dot{\tilde{\boldsymbol{q}}})\right) \geq 0$ must be fulfilled for any $t, \boldsymbol{\eta}, \tilde{\boldsymbol{q}}$ and $\dot{\tilde{\boldsymbol{q}}}$, cf.* (38).

B. Coordinate Transformation

Note, that the link-side of the new system (37) behaves like the original system (1) without gravity but with additional damping and tracking properties. We introduce new motor coordinates that reflect this behavior. To this end, we impose equivalence of (1) and (37) to find an implicit relation

$$\boldsymbol{\psi}(\boldsymbol{\theta} - \boldsymbol{q}) = \boldsymbol{\psi}(\boldsymbol{\eta} - \tilde{\boldsymbol{q}}) + \boldsymbol{n}(t, \tilde{\boldsymbol{q}}, \dot{\tilde{\boldsymbol{q}}}) \tag{38}$$

between the new motor coordinates $\boldsymbol{\eta}$ and the original system states $\boldsymbol{\theta}, \boldsymbol{q}$ of (1)-(2), where

$$\boldsymbol{n}(t, \tilde{\boldsymbol{q}}, \dot{\tilde{\boldsymbol{q}}}) := \boldsymbol{g}(t, \tilde{\boldsymbol{q}}) - \boldsymbol{D}\dot{\tilde{\boldsymbol{q}}} + \boldsymbol{M}(t, \tilde{\boldsymbol{q}})\ddot{\boldsymbol{q}}_d(t) + \boldsymbol{C}(t, \tilde{\boldsymbol{q}}, \dot{\tilde{\boldsymbol{q}}})\dot{\boldsymbol{q}}_d(t). \tag{39}$$

Since the inverse of $\boldsymbol{\psi}$ is usually not analytically available, (38) cannot be solved directly and $\boldsymbol{\eta}$ has to be determined numerically.[12] Differentiating (38) with respect to time gives us a differential relation between the old and new motor coordinates[13]

$$\boldsymbol{\kappa}(\boldsymbol{\theta} - \boldsymbol{q})(\dot{\boldsymbol{\theta}} - \dot{\boldsymbol{q}}) = \boldsymbol{\kappa}(\boldsymbol{\eta} - \tilde{\boldsymbol{q}})(\dot{\boldsymbol{\eta}} - \dot{\tilde{\boldsymbol{q}}}) + \dot{\boldsymbol{n}}(t, \tilde{\boldsymbol{q}}, \dot{\tilde{\boldsymbol{q}}}). \tag{40}$$

See (5) for the definition of $\boldsymbol{\kappa}$. Solving (40) for $\dot{\boldsymbol{\theta}}$ gives us[14]

$$\begin{aligned}\dot{\boldsymbol{\theta}} = {} & \boldsymbol{\kappa}^{-1}(\boldsymbol{\theta} - \boldsymbol{q})\boldsymbol{\kappa}(\boldsymbol{\eta} - \tilde{\boldsymbol{q}})\dot{\boldsymbol{\eta}} + \dot{\tilde{\boldsymbol{q}}} + \dot{\boldsymbol{q}}_d(t) \\ & + \boldsymbol{\kappa}^{-1}(\boldsymbol{\theta} - \boldsymbol{q})\boldsymbol{\gamma}(t, \boldsymbol{\eta}, \tilde{\boldsymbol{q}}, \dot{\tilde{\boldsymbol{q}}}, \ddot{\tilde{\boldsymbol{q}}}),\end{aligned} \tag{41}$$

where

$$\boldsymbol{\gamma}(t, \boldsymbol{\eta}, \tilde{\boldsymbol{q}}, \dot{\tilde{\boldsymbol{q}}}, \ddot{\tilde{\boldsymbol{q}}}) := -\boldsymbol{\kappa}(\boldsymbol{\eta} - \tilde{\boldsymbol{q}})\ddot{\tilde{\boldsymbol{q}}} + \dot{\boldsymbol{n}}(t, \tilde{\boldsymbol{q}}, \dot{\tilde{\boldsymbol{q}}}). \tag{42}$$

With (38), we can re-write $\dot{\boldsymbol{\theta}}$ as a function of the new states only

$$\dot{\boldsymbol{\theta}} = \boldsymbol{A}(t, \boldsymbol{\eta}, \tilde{\boldsymbol{q}}, \dot{\tilde{\boldsymbol{q}}})\dot{\boldsymbol{\eta}} + \boldsymbol{a}(t, \boldsymbol{\eta}, \tilde{\boldsymbol{q}}, \dot{\tilde{\boldsymbol{q}}}, \ddot{\tilde{\boldsymbol{q}}}). \tag{43}$$

[12]For the implementation in our robot system we use fixed point iteration.

[13]Higher derivatives of $\boldsymbol{q}$, such as $\ddot{\boldsymbol{q}}$ and $\boldsymbol{q}^{(3)}$, are calculated based on the model of the plant. In the end, the controller solely depends on $[\boldsymbol{\eta}, \tilde{\boldsymbol{q}}]$ and $[\dot{\boldsymbol{\eta}}, \dot{\tilde{\boldsymbol{q}}}]$. In order to better understand which terms depend in the first instance on higher derivatives, we do not make these substitutions.

[14]The singular values of $\boldsymbol{\kappa}(\boldsymbol{\phi})$ are bounded and bounded away from zero. Thus, $\boldsymbol{\kappa}^{-1}$ exists and is again bounded.

See Appendix for $\boldsymbol{A}$ and $\boldsymbol{a}$. Differentiating (43) with respect to time yields

$$\ddot{\boldsymbol{\theta}} = \boldsymbol{A}(t, \boldsymbol{\eta}, \tilde{\boldsymbol{q}}, \dot{\tilde{\boldsymbol{q}}})\ddot{\boldsymbol{\eta}} + \dot{\boldsymbol{A}}(t, \boldsymbol{\eta}, \tilde{\boldsymbol{q}}, \dot{\tilde{\boldsymbol{q}}})\dot{\boldsymbol{\eta}} + \dot{\boldsymbol{a}}(t, \boldsymbol{\eta}, \tilde{\boldsymbol{q}}, \dot{\tilde{\boldsymbol{q}}}, \ddot{\tilde{\boldsymbol{q}}}). \tag{44}$$

The relations (38) and (44) allow us to perform a coordinate transformation $[\boldsymbol{\theta}, \boldsymbol{q}] \mapsto [\boldsymbol{\eta}, \tilde{\boldsymbol{q}}]$ for the robot dynamics (1)-(2). Obviously, for the link dynamics we yield the desired dynamics (37). For the transformed motor dynamics we get

$$\boldsymbol{B}\boldsymbol{A}\ddot{\boldsymbol{\eta}} + \boldsymbol{B}\dot{\boldsymbol{A}}\dot{\boldsymbol{\eta}} + \boldsymbol{B}\dot{\boldsymbol{a}} + \boldsymbol{\psi}(\boldsymbol{\theta} - \boldsymbol{q}) = \boldsymbol{u} \tag{45}$$

Based on the transformed dynamics we introduce two control approaches which differ on the achieved closed-loop motor dynamics. Both approaches have in common that they preserve the link-side inertial properties and the elastic structure of the original plant dynamics. Apart from that, ESP control focuses on preserving the inertial properties of motor dynamics (see Sec. IV-C). While ESP+ control aims at minimizing the dynamic shaping on the motor side (see Sec. IV-D).

C. ESP Control

We design the controller in three steps, such that the resulting controller $\boldsymbol{u} = \boldsymbol{u}_{\text{ESP}}$ is composed of three components

$$\boldsymbol{u}_{\text{ESP}} := \check{\boldsymbol{u}}_{\text{ESP}} + \hat{\boldsymbol{u}}_{\text{ESP}} + \bar{\boldsymbol{u}}_{\text{ESP}}. \tag{46}$$

First, we pre-compensate some nonlinear terms by

$$\check{\boldsymbol{u}}_{\text{ESP}} = \boldsymbol{B}\left(\dot{\boldsymbol{A}}\dot{\boldsymbol{\eta}} + \dot{\boldsymbol{a}}\right), \tag{47}$$

resulting in the following intermediary dynamics

$$\boldsymbol{B}\boldsymbol{A}\ddot{\boldsymbol{\eta}} + \boldsymbol{\psi}(\boldsymbol{\theta} - \boldsymbol{q}) = \hat{\boldsymbol{u}}_{\text{ESP}} + \check{\boldsymbol{u}}_{\text{ESP}}. \tag{48}$$

Second, we shape the motor inertia such that the original, constant motor inertia $\boldsymbol{B}$ results. In addition, we transform the spring torques into the new coordinates. Clearly,

$$\hat{\boldsymbol{u}}_{\text{ESP}} = \boldsymbol{\psi}(\boldsymbol{\theta} - \boldsymbol{q}) - \boldsymbol{B}\boldsymbol{A}\boldsymbol{B}^{-1}\boldsymbol{\psi}(\boldsymbol{\eta} - \tilde{\boldsymbol{q}}) \tag{49}$$

yields the intermediary dynamics

$$\boldsymbol{B}\ddot{\boldsymbol{\eta}} + \boldsymbol{\psi}(\boldsymbol{\eta} - \tilde{\boldsymbol{q}}) = \boldsymbol{B}\boldsymbol{A}^{-1}\boldsymbol{B}^{-1}\bar{\boldsymbol{u}}_{\text{ESP}}. \tag{50}$$

At last, we choose PD control in the new motor coordinates

$$\bar{\boldsymbol{u}}_{\text{ESP}} = -\boldsymbol{B}\boldsymbol{A}\boldsymbol{B}^{-1}(\boldsymbol{K}_D\dot{\boldsymbol{\eta}} + \boldsymbol{K}_P\boldsymbol{\eta}). \tag{51}$$

to achieve link-side motion tracking. In the end, we yield the following closed-loop motor dynamics

$$\boldsymbol{B}\ddot{\boldsymbol{\eta}} + \boldsymbol{\psi}(\boldsymbol{\eta} - \tilde{\boldsymbol{q}}) = -\boldsymbol{K}_D\dot{\boldsymbol{\eta}} - \boldsymbol{K}_P\boldsymbol{\eta}. \tag{52}$$

Fig. 7 presents the block-diagram that corresponds to the ESP control law. For the PD gains we assume:

Assumption 5. *$\boldsymbol{K}_P, \boldsymbol{K}_D \in \mathbb{R}^{n\times n}$ are bounded, symmetric and positive definite. Note, that $\boldsymbol{K}_D$ can also be a function of the states $\boldsymbol{\eta}, \tilde{\boldsymbol{q}}$.*

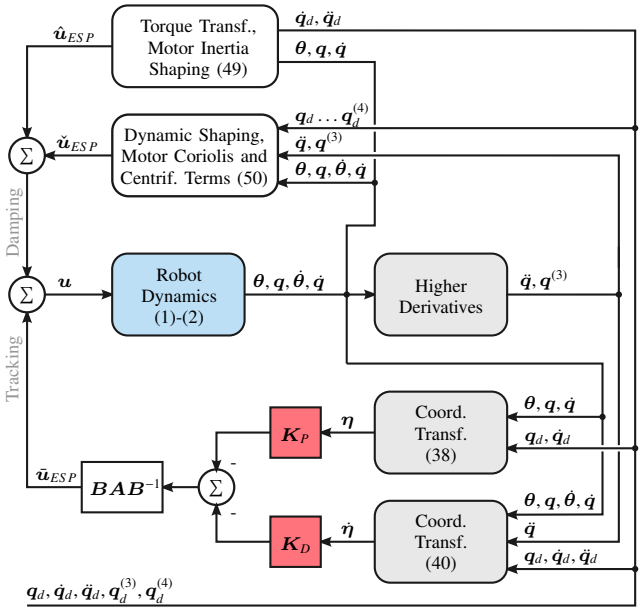

Fig. 7. ESP control scheme.

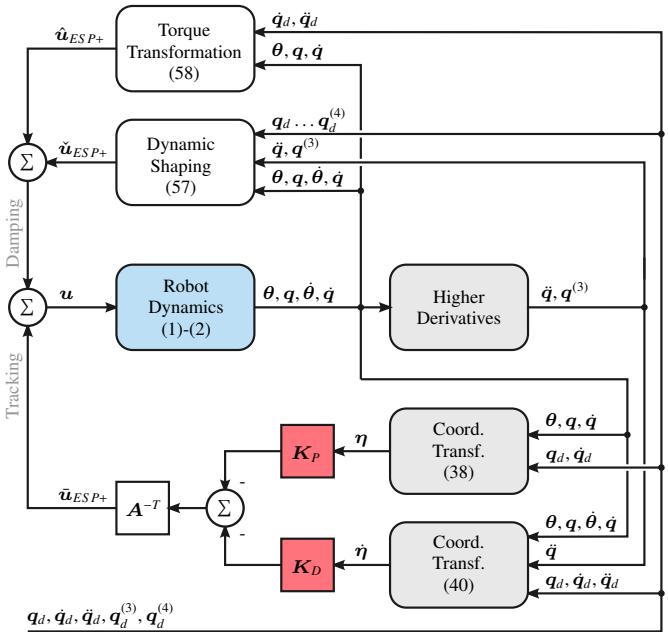

Fig. 8. ESP+ control scheme.

D. ESP+ Control

Pre-multiplying (45) by $\boldsymbol{A}^{\mathrm{T}}$ yields the following transformed motor dynamics

$$\boldsymbol{B}_\eta \ddot{\boldsymbol{\eta}} + \boldsymbol{C}_\eta \dot{\boldsymbol{\eta}} + \boldsymbol{A}^{\mathrm{T}} \psi(\boldsymbol{\theta} - \boldsymbol{q}) + \boldsymbol{A}^{\mathrm{T}} \boldsymbol{B} \dot{\boldsymbol{a}} = \boldsymbol{A}^{\mathrm{T}} \boldsymbol{u}, \tag{53}$$

where

$$\boldsymbol{B}_\eta(t, \boldsymbol{\eta}, \tilde{\boldsymbol{q}}, \dot{\tilde{\boldsymbol{q}}}) \coloneqq \boldsymbol{A}^{\mathrm{T}}(t, \boldsymbol{\eta}, \tilde{\boldsymbol{q}}, \dot{\tilde{\boldsymbol{q}}}) \boldsymbol{B} \boldsymbol{A}(t, \boldsymbol{\eta}, \tilde{\boldsymbol{q}}, \dot{\tilde{\boldsymbol{q}}}) \tag{54}$$

and

$$\boldsymbol{C}_\eta(t, \boldsymbol{\eta}, \dot{\boldsymbol{\eta}}, \tilde{\boldsymbol{q}}, \dot{\tilde{\boldsymbol{q}}}, \ddot{\tilde{\boldsymbol{q}}}) \coloneqq \boldsymbol{A}^{\mathrm{T}}(t, \boldsymbol{\eta}, \tilde{\boldsymbol{q}}, \dot{\tilde{\boldsymbol{q}}}) \boldsymbol{B} \dot{\boldsymbol{A}}(t, \boldsymbol{\eta}, \tilde{\boldsymbol{q}}, \dot{\tilde{\boldsymbol{q}}}) \tag{55}$$

can be considered as naturally arising inertia and Coriolis/centrifugal matrices, respectively. Compared to the ESP approach, we keep the Coriolis/centrifugal terms and refrain from shaping the motor inertia. Again, we derive the control law in three steps, such that the resulting control input $\boldsymbol{u} = \boldsymbol{u}_{ESP+}$ is composed of three components

$$\boldsymbol{u}_{ESP+} \coloneqq \check{\boldsymbol{u}}_{ESP+} + \hat{\boldsymbol{u}}_{ESP+} + \bar{\boldsymbol{u}}_{ESP+}. \tag{56}$$

We start by canceling some nonlinear terms by

$$\check{\boldsymbol{u}}_{ESP+} \coloneqq \boldsymbol{B} \dot{\boldsymbol{a}}. \tag{57}$$

We proceed with transforming the spring torques into the new coordinates

$$\hat{\boldsymbol{u}}_{ESP+} \coloneqq \psi(\boldsymbol{\theta} - \boldsymbol{q}) - \boldsymbol{A}^{-T} \psi(\boldsymbol{\eta} - \tilde{\boldsymbol{q}}). \tag{58}$$

Finally, we choose PD control in the new coordinates

$$\bar{\boldsymbol{u}}_{ESP+} \coloneqq -\boldsymbol{A}^{-T}(\boldsymbol{K}_D \dot{\boldsymbol{\eta}} + \boldsymbol{K}_P \boldsymbol{\eta}). \tag{59}$$

to achieve link-side tracking behavior. In the end, the following closed-loop motor dynamics

$$\boldsymbol{B}_\eta \ddot{\boldsymbol{\eta}} + \boldsymbol{C}_\eta \dot{\boldsymbol{\eta}} + \psi(\boldsymbol{\eta} - \tilde{\boldsymbol{q}}) = -\boldsymbol{K}_D \dot{\boldsymbol{\eta}} - \boldsymbol{K}_P \boldsymbol{\eta} \tag{60}$$

results. For $\boldsymbol{K}_D$ and $\boldsymbol{K}_P$ we make the same assumptions as above. Fig. 8 depicts the block-diagram that corresponds to the ESP+ control law.

Through the coordinate transformation, state-dependent virtual mass and Coriolis matrices naturally arise on the controlled motor side. The resulting closed-loop dynamics have some beneficial properties, such as the skew-symmetry of $\dot{\boldsymbol{B}}_\eta - 2\boldsymbol{C}_\eta$, which will be exploited later in the stability proof. Physically, this can be interpreted as energy conservation properties of the motors, i.e., the time derivative of the total virtual kinetic energy $\frac{1}{2}\dot{\boldsymbol{\eta}}^{\mathrm{T}} \boldsymbol{B}_\eta \dot{\boldsymbol{\eta}}$ of the motors[15] is equal to the virtual power provided by the springs $\psi(\boldsymbol{\eta} - \boldsymbol{q})$ and the PD control input $\bar{\boldsymbol{u}}$

$$\frac{1}{2}\frac{\mathrm{d}}{\mathrm{d}t}(\dot{\boldsymbol{\eta}}^{\mathrm{T}} \boldsymbol{B}_\eta \dot{\boldsymbol{\eta}}) = \dot{\boldsymbol{\eta}}^{\mathrm{T}}(-\psi(\boldsymbol{\eta} - \tilde{\boldsymbol{q}}) + \bar{\boldsymbol{u}}). \tag{61}$$

By observing

$$\boldsymbol{B} = \boldsymbol{B}^{\mathrm{T}} \implies \dot{\boldsymbol{B}}_\eta = \dot{\boldsymbol{A}}^{\mathrm{T}} \boldsymbol{B} \boldsymbol{A} + \boldsymbol{A}^{\mathrm{T}} \boldsymbol{B} \dot{\boldsymbol{A}} = \boldsymbol{C}_\eta^{\mathrm{T}} + \boldsymbol{C}_\eta, \tag{62}$$

one can easily show the skew symmetry of $\dot{\boldsymbol{B}}_\eta - 2\boldsymbol{C}_\eta$

$$\begin{aligned} \dot{\boldsymbol{\eta}}^{\mathrm{T}}(\dot{\boldsymbol{B}}_\eta - 2\boldsymbol{C}_\eta)\dot{\boldsymbol{\eta}} &= \dot{\boldsymbol{\eta}}^{\mathrm{T}}(\boldsymbol{C}_\eta^{\mathrm{T}} - \boldsymbol{C}_\eta)\dot{\boldsymbol{\eta}} = \dot{\boldsymbol{\eta}}^{\mathrm{T}}(-\boldsymbol{C}_\eta^{\mathrm{T}} + \boldsymbol{C}_\eta)^{\mathrm{T}}\dot{\boldsymbol{\eta}} \\ &= -\dot{\boldsymbol{\eta}}^{\mathrm{T}}(\boldsymbol{C}_\eta^{\mathrm{T}} - \boldsymbol{C}_\eta)^{\mathrm{T}}\dot{\boldsymbol{\eta}}. \end{aligned} \tag{63}$$

$\boldsymbol{B}_\eta$ also shares the symmetry and positive definiteness with standard mass matrices. Latter can be shown by establishing a lower bound for the eigenvalues of $\boldsymbol{B}_\eta$. We can write $\boldsymbol{B}_\eta$ as product of two positive definite Hermitian matrices and by applying repetitively Lemma 2 we get

$$\begin{aligned} \underline{\lambda}^2\left(\boldsymbol{B}_\eta\right) &\geq \underline{\lambda}\left(\boldsymbol{A}^{\mathrm{T}}\boldsymbol{B}^{1/2}\right)\underline{\lambda}\left((\boldsymbol{A}^{\mathrm{T}}\boldsymbol{B}^{1/2})^{\mathrm{T}}\right) \\ &\geq \underline{\lambda}^2\left(\boldsymbol{A}^{\mathrm{T}}\boldsymbol{B}^{1/2}\right) \geq \underline{\lambda}^2(\boldsymbol{A})\,\underline{\lambda}(\boldsymbol{B}) > 0. \end{aligned} \tag{64}$$

[15]The positive definiteness of $\boldsymbol{B}_\eta$ is shown at the end of this section.

For that $\boldsymbol{A}$, $\boldsymbol{B}$ and $\boldsymbol{B}^{1/2}$ have to be Hermitian and non-negative. Since $\boldsymbol{\kappa}$ is derived from a positive definite potential function, see Ass. 1, we know that that $\boldsymbol{\kappa}$, and therefore $\boldsymbol{A}$, are symmetric and positive definite.[16] From Property 1, the same can be shown for both $\boldsymbol{B}$ and $\boldsymbol{B}^{1/2}$.

E. A Discussion of the ESP and ESP+ controllers

In both cases, we modified the link dynamics to the same minimum extent, kept the structure and elastic coupling of the original dynamics intact and added only tracking terms. In each case, the closed-loop system can be interpreted as a multi-spring-damper system – it can be thought of as an n-link chain where each link is compromised of an element shown in Fig. 2(d). Thereby, the passivity property is obviously retained (see Sec. V for details) and it allows us to find a physically motivated, virtual energy-based Lyapunov function for the stability proof (see Sec. VI for details). The ESP+ controller extends the concept of minimizing the dynamical shaping to the motor side, by keeping the naturally arising inertia, Coriolis- and centrifugal terms, therefore the extra '+' in its name.[17]

Observe, that in both cases the PD control terms are state-dependent and model-based.[18] Note, that $\bar{u}_{\text{ESP}}$ contains $\boldsymbol{A}^{-T}$, while $\bar{u}_{ESP+}$ contains $\boldsymbol{BAB}^{-1}$. More about how these differences manifest in practice follows in Sec. VII.

For linear elasticities, with some constant stiffness $\boldsymbol{K} \in \mathbb{R}^{n\times n}$, such that $\boldsymbol{\kappa}(\boldsymbol{\phi}) = \boldsymbol{K}\boldsymbol{\phi}$, ESP and ESP+ control are equivalent, and we simply refer to it by the name ESP control. The resulting control law is significantly shorter. Figure 9 presents the corresponding block diagram. Interestingly, the pure damping part of the controller ($\hat{\boldsymbol{u}} + \check{\boldsymbol{u}}$) does not rely on measurement of the motor positions or their time derivatives. The measured link positions and velocities only come into play via the inertia, Coriolis-/centrifugal and gravity terms as part of the pseudo-feedforward torque $\boldsymbol{n}$.

In general, opposing to feedback linearization, no compensation of the centrifugal and Coriolis terms is performed.

F. Quasi-rigid Manipulators

Interestingly, for the 'quasi-rigid' limit case, that is, when the stiffness approaches infinitely large values, i.e. $\underline{\sigma}(\boldsymbol{\kappa}) \to \infty$, both, the ESP and ESP+ controller result in the popular PD+ controller [27]. For the case of nonlinear elasticities we spare the straightforward, but cumbersome computations to show this. In case of linear elasticities, the calculations simplify significantly. In fact, we can draw conclusions for the transition to the 'quasi-rigid' case, simply by analyzing the corresponding block diagram in Fig. 9 under the assumption $\boldsymbol{K}^{-1} \to \boldsymbol{0}$.

[16]Note, the inverse of a symmetric, p.d. matrix is also symmetric, p.d. and and the product of two Hermitian matrices p.d. is again p.d..

[17]The '+' was chosen with regard to the analogy to the PD+ control, for which the original Coriolis and inertia matrices are present in the closed-loop error dynamics.

[18]The state-dependence come into play via $\boldsymbol{A}(t, \boldsymbol{\eta}, \tilde{\boldsymbol{q}}, \dot{\tilde{\boldsymbol{q}}})$. The calculations of $\boldsymbol{\eta}$ and $\dot{\boldsymbol{\eta}}$ explicitly require terms from the model of the robot.

V. Passivity Analysis

In this section we analyze the passivity properties for the time-variant closed-loop dynamics (37), (60).[19]

$$\boldsymbol{M}(t, \tilde{\boldsymbol{q}})\ddot{\tilde{\boldsymbol{q}}} + \boldsymbol{C}(t, \tilde{\boldsymbol{q}}, \dot{\tilde{\boldsymbol{q}}})\dot{\tilde{\boldsymbol{q}}} = -\boldsymbol{D}\dot{\tilde{\boldsymbol{q}}} + \boldsymbol{\psi}(\boldsymbol{\eta} - \tilde{\boldsymbol{q}}) + \boldsymbol{\tau}_{ext}, \tag{65}$$

$$\begin{aligned}\boldsymbol{B}_\eta(t, \boldsymbol{\eta}, \tilde{\boldsymbol{q}}, \dot{\tilde{\boldsymbol{q}}})\dot{\boldsymbol{\eta}} + \boldsymbol{C}_\eta(t, \boldsymbol{\eta}, \dot{\boldsymbol{\eta}}, \tilde{\boldsymbol{q}}, \dot{\tilde{\boldsymbol{q}}}, \ddot{\tilde{\boldsymbol{q}}})\dot{\boldsymbol{\eta}} + \boldsymbol{\psi}(\boldsymbol{\eta} - \tilde{\boldsymbol{q}}) \\ = -\boldsymbol{K}_D\dot{\boldsymbol{\eta}} - \boldsymbol{K}_P\boldsymbol{\eta}.\end{aligned} \tag{66}$$

Remark 3. The ESP control related closed-loop dynamics (65), (52) can be considered as a special case of the ESP+ control related closed-loop dynamics given above, with constant motor inertia $\boldsymbol{B}_\eta = \boldsymbol{B}$ and $\boldsymbol{C}_\eta = \boldsymbol{0}$. As such, it is sufficient to deduce passivity and stability (see Sec. VI) statements for the latter.

We prove that the link-side dynamics (65) and motor dynamics (66) of the closed-loop system can be interpreted as an interconnection of passive subsystems, see Fig. 10. According to the definition in [31], we have to show that for any period of time, the system cannot output more virtual energy at its ports of interaction than has in total been injected into for that period of time and has initially been stored. With Fig. 2(d) in mind, it is natural to choose

$$S_{\tilde{q}} := \frac{1}{2}\dot{\tilde{\boldsymbol{q}}}^{\mathrm{T}}\boldsymbol{M}(t, \tilde{\boldsymbol{q}})\dot{\tilde{\boldsymbol{q}}} \tag{67}$$

as storage function for the closed-loop link-side dynamics (65) and

$$S_\eta := \frac{1}{2}\dot{\boldsymbol{\eta}}^{\mathrm{T}}\boldsymbol{B}_\eta(t, \boldsymbol{\eta}, \tilde{\boldsymbol{q}}, \dot{\tilde{\boldsymbol{q}}})\dot{\boldsymbol{\eta}} + U_s(\boldsymbol{\eta} - \tilde{\boldsymbol{q}}) + \frac{1}{2}\boldsymbol{\eta}^{\mathrm{T}}\boldsymbol{K}_P\boldsymbol{\eta}, \tag{68}$$

as storage function for the closed-loop motor dynamics (66). Eq. (67) represents the virtual kinetic energy of the link. Accordingly, the first term on the RHS in (68) represents the virtual kinetic energy of the controlled motor. The other two terms can be interpreted as the potential energy of the spring and a virtual potential energy of the control, respectively.

For the analysis of the passivity properties, we express the time derivative of (67) along the solutions of (65). By exploiting Prop. 3 we get

$$\dot{S}_{\tilde{q}} = -\dot{\tilde{\boldsymbol{q}}}^{\mathrm{T}}\boldsymbol{D}\dot{\tilde{\boldsymbol{q}}} + \dot{\tilde{\boldsymbol{q}}}^{\mathrm{T}}\boldsymbol{\psi}(\boldsymbol{\eta} - \tilde{\boldsymbol{q}}) + \dot{\tilde{\boldsymbol{q}}}^{\mathrm{T}}\boldsymbol{\tau}_{ext}. \tag{69}$$

We can identify three terms in (69). The first one represents the dissipation of energy due to the damping assignment on the link side. The latter two are corresponding to an interconnection port with the closed-loop motor dynamics and the environment, respectively. As visualized in Fig. 10, $\dot{\tilde{\boldsymbol{q}}}^{\mathrm{T}}\boldsymbol{\psi}(\boldsymbol{\eta} - \tilde{\boldsymbol{q}})$ represents the interconnection with the motor side and $\dot{\tilde{\boldsymbol{q}}}^{\mathrm{T}}\boldsymbol{\tau}_{ext}$ represents the interconnection with the environment. Correspondingly, by exploiting the skew symmetry of $\dot{\boldsymbol{B}}_\eta - 2\boldsymbol{C}_\eta$, we can write the time derivative of (67) as follows

$$\dot{S}_\eta = -\dot{\boldsymbol{\eta}}^{\mathrm{T}}\boldsymbol{K}_D\dot{\boldsymbol{\eta}} - \dot{\tilde{\boldsymbol{q}}}^{\mathrm{T}}\boldsymbol{\psi}(\boldsymbol{\eta} - \tilde{\boldsymbol{q}}). \tag{70}$$

Again, we can identify a dissipation term. This term is related to the introduced damping on the motor side. The interconnection term between link and motor dynamics also appears again (cf. (69)). The analysis so far motivates the following proposition:

[19]Recall, the coordinate transformation (38) imposes equality of (1) and (37).

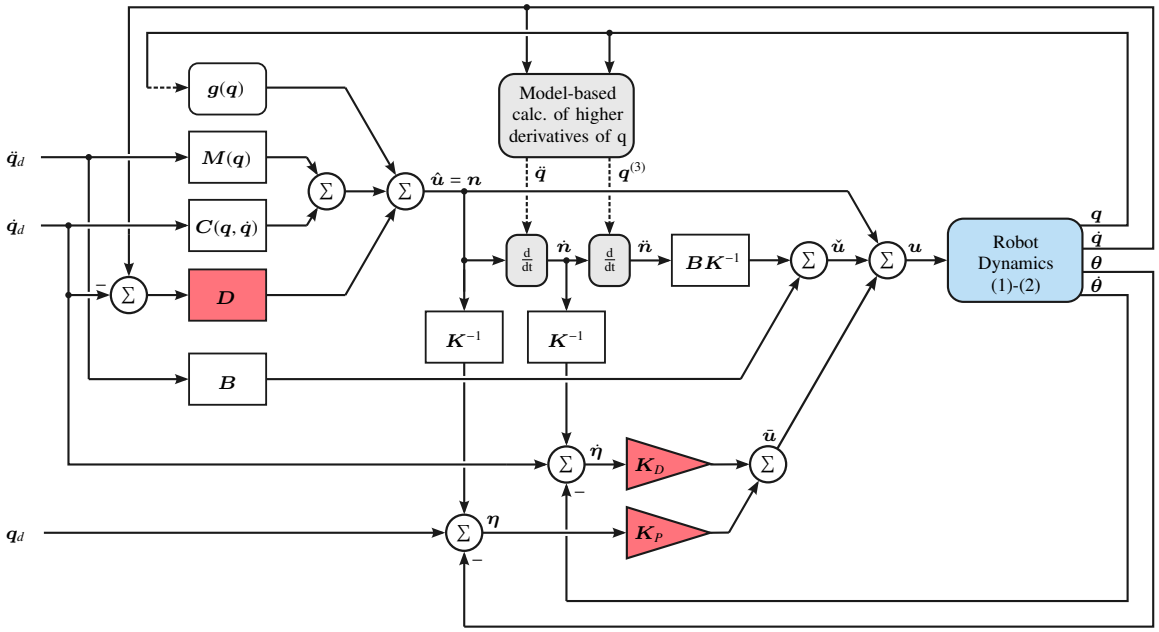

Fig. 9. ESP control scheme for linear springs. Note, the 'd/dt' blocks indicate analytical differentiation of the input signal, therefore yielding the first and second time derivative of $\boldsymbol{n}$ (cf. (39)). This requires up to the third-order time-derivatives of $\boldsymbol{q}$ as indicated by the dotted arrows. Recall, that all time-derivates of higher higher order than one are computed model based in a real implementation.

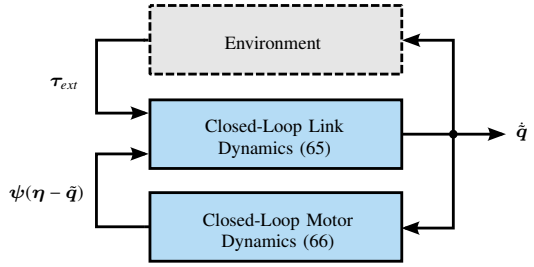

Fig. 10. The closed-loop dynamics (65)-(66) can be represented as an interconnection of passive subsystems. For the tracking case the link side interacts with the motor side via the power port $\dot{\tilde{\boldsymbol{q}}}^{\mathrm{T}}\boldsymbol{\psi}(\boldsymbol{\eta}-\tilde{\boldsymbol{q}})$ and with a passive environment via the power port $\dot{\tilde{\boldsymbol{q}}}^{\mathrm{T}}\boldsymbol{\tau}_{ext}$.

Proposition 1. *The closed-loop system* (65)-(66) *represents a passive map from the generalized external forces* $\boldsymbol{\tau}_{ext}$ *to the generalized velocities of the link-side tracking error* $\dot{\tilde{\boldsymbol{q}}}$.

Proof. Consider the storage function $S = S_{\tilde{q}} + S_{\eta}$ comprising (67) and (68). Its time derivative is given by the sum of (69) and (70)

$$\dot{S} = -\dot{\tilde{\boldsymbol{q}}}^{\mathrm{T}}\boldsymbol{D}\dot{\tilde{\boldsymbol{q}}} + \dot{\tilde{\boldsymbol{q}}}\boldsymbol{\tau}_{ext} - \dot{\boldsymbol{\eta}}^{\mathrm{T}}\boldsymbol{K}_D\dot{\boldsymbol{\eta}} \leq \dot{\tilde{\boldsymbol{q}}}^{\mathrm{T}}\boldsymbol{\tau}_{ext}, \tag{71}$$

which completes the proof. □

Note that for the regulation case passivity with respect to the physically more intuitive power port $\dot{\boldsymbol{q}}, \boldsymbol{\tau}_{ext}$ is given. Nevertheless, situations may arise in practice where passivity with respect to the power port $\dot{\tilde{\boldsymbol{q}}}, \boldsymbol{\tau}_{ext}$ will be of importance. More specifically, there exist situations where the environment or the interacting object move synchronously to the link reference trajectory. One such scenario would be object manipulation on a conveyor belt. In that case, the proposed tracking controlled robot would passively interact with the object.

VI. Stability Analysis

In this section we analyze the stability properties for the time-variant closed-loop dynamics (65)-(66). First, we formulate the main result of the paper in form of the following theorem.

Theorem 1. *Consider the closed-loop dynamics* (65)-(66) *in absence of external, generalized forces* $\boldsymbol{\tau}_{ext}$. *Under the assumptions made in Sec. II, the origin of the closed-loop system is uniformly globally asymptotically stable.*

The proof of Theorem 1 relies on Lyapunov theory and exploits Matrosov's Theorem [32]. For convenience, it is given below. Consider the differential equation

$$\dot{\boldsymbol{x}} = \boldsymbol{f}(t, \boldsymbol{x}), \tag{72}$$

where $\boldsymbol{x} \in \mathbb{R}^n$, $t \in \mathbb{R}$ is the time and $\boldsymbol{f}$ is a continuous function $\boldsymbol{f} : I \times \Omega \to \mathbb{R}^n$, where $I = [t_0, \infty)$ for some $t_0 \in \mathbb{R}$ and Ω is an open connected set in $\mathbb{R}^n$, containing the origin. We assume that $\boldsymbol{f}(t, \boldsymbol{0}) = \boldsymbol{0} \quad \forall t \in I$, so that the origin is an equilibrium point for the differential equation (72). Matrosov's theorem then states:

Matrosov's Theorem (Rouche [32])**.** *Let there there exist two* C^1 *functions* $V : I \times \Omega \to \mathbb{R}$, $W : I \times \Omega \to \mathbb{R}$, *a* C^0 *function* $V^* : \Omega \to \mathbb{R}$, *three functions* a, b, c *of class* $\mathcal{K}$ *and two constants* $S > 0$ *and* $T > 0$ *such that, for every* $(t, x) \in I \times \Omega$

(i) $a(\|\boldsymbol{x}\|) \leq V(t, \boldsymbol{x}) \leq b(\|\boldsymbol{x}\|)$;
(ii) $\dot{V}(t, \boldsymbol{x}) \leq V^*(\boldsymbol{x}) \leq 0$; $E := \{\boldsymbol{x} \in \Omega : V^*(\boldsymbol{x}) = 0\}$;
(iii) $|W(t, \boldsymbol{x})| < S$;
(iv) $\max(d(\boldsymbol{x}, E), |\dot{W}(t, \boldsymbol{x})|) \geq c(\|\boldsymbol{x}\|)$ [20];
(v) $\|\boldsymbol{f}(t, \boldsymbol{x})\| < T$;

[20] $d(\boldsymbol{x}, E)$ is the minimum distance of point $\boldsymbol{x}$ to set E, i.e. $\inf_{\boldsymbol{y} \in E}(\|\boldsymbol{x} - \boldsymbol{y}\|)$

choosing $\alpha > 0$ such that $\bar{B}_\alpha \subset \Omega$, let us put for every $t \in I$

$$V_{t,\alpha}^{-1} = \boldsymbol{x} \in \Omega : V(t, \boldsymbol{x}) \leq a(\alpha). \tag{73}$$

Then

(i) *for any $t_0 \in I$ and any $\boldsymbol{x}_0 \in V_{t_0,\alpha}^{-1}$, any solution $\boldsymbol{x}(t)$ of (72), passing through $(\boldsymbol{x}_0, t_0) \in I \times \Omega$, tends to zero uniformly in t_0 and $\boldsymbol{x}_0$, as $t \to \infty$.*

(ii) *the origin is uniformly asymptotically stable.*

The foundations for this theorem were published in [33]. What is interesting about this theorem is that it states conditions under which a Lyapunov function with negative semi-definite time derivative is sufficient to proof asymptotic stability. Its central idea relies on the appealing usage of a bounded auxiliary function that ensures that the system cannot get stuck in the problematic set where the time-derivative of the Lyapunov function is zero.

In order to facilitate the verification of condition (iv) we apply the following lemma by Paden and Panja

Lemma 1 (B. Paden, R. Panja, [27])**.**
Condition (iv) *of Matrosov's theorem is satisfied if conditions below are satisfied.*

(iv.a) *$\dot{W}(\boldsymbol{x}, t)$ is continuous in both arguments and depends on time in the following way. $\dot{W}(\boldsymbol{x}, t) = g(\boldsymbol{x}, \beta(t))$ where g is continuous in both of its arguments. $\beta(t)$ is also continuous and its image lies in a bounded set K_1. (For simplicity, we assume that $\dot{W}(\boldsymbol{x}, t)$ depends on time continuously through a bounded function.)*

(iv.b) *There exists a class $\mathcal{K}$ function, k, such that $|\dot{W}(\boldsymbol{x}, t)| \geq k(\|\boldsymbol{x}\|) \forall \boldsymbol{x} \in E$ and $t \geq t_0$.*

For a proof see [27].

A. Proof of the Main Result (Theorem 1)

It is sufficient to check the conditions of Matrosov's Theorem. Most of the computations are straight forward, but become tedious at times. This is especially true for the part that checks condition (iv.a) of Lemma 1. In general, the proof relies heavily on the application of the boundedness theorem, Lemma 2 and matrix norm properties.

For better readability we will neglect the arguments of $\boldsymbol{M}, \boldsymbol{C}, \boldsymbol{D}, \boldsymbol{B}_\eta$ and $\boldsymbol{C}_\eta$ if they are not beneficial to promote understanding. The states are summarized into a new state vector $\boldsymbol{x} := [\boldsymbol{\eta}, \dot{\boldsymbol{\eta}}, \boldsymbol{q}, \dot{\boldsymbol{q}}]^{\mathrm{T}}$. Consider the following energy based, time-variant, Lyapunov function candidate $V : [0, \infty) \times \Omega \to \mathbb{R}$

$$V(t, \boldsymbol{x}) = S_{\tilde{q}}(t, \boldsymbol{q}, \dot{\boldsymbol{q}}) + S_\eta(t, \boldsymbol{\eta}, \dot{\boldsymbol{\eta}}, \boldsymbol{q}) \tag{74}$$

For now, Ω can be chosen arbitrarily large. Obviously, V is lower bounded since $\boldsymbol{M}, \boldsymbol{B}_\eta, \boldsymbol{K}_P$ and the spring potential U_s are positive definite matrices and functions, respectively (cf. Prop. 2, Ass. 1 and Ass. 5). Thus, in fact, V is positive definite in $\boldsymbol{x}$. Later in the text, V is required to be at least three times continuously differentiable. From (71) we have

$$\dot{V}(t, \boldsymbol{x}) = -\dot{\tilde{\boldsymbol{q}}}^{\mathrm{T}} \boldsymbol{D} \dot{\tilde{\boldsymbol{q}}} - \dot{\boldsymbol{\eta}}^{\mathrm{T}} \boldsymbol{K}_D \dot{\boldsymbol{\eta}}. \tag{75}$$

$\dot{V}$ is negative semi-definite due to the positive definiteness of $\boldsymbol{K}_D$ and $\boldsymbol{D}$. Thus, V is a Lyapunov function of (65)–(66).

Ad Cond. (i) of Matrosov's Theorem: Clearly, condition (i) of Matrosov's Theorem can be satisfied by choosing upper and lower bounds for V as follows

$$\alpha(\boldsymbol{x}) = \frac{1}{2}\left(\underline{\lambda}(\boldsymbol{M})\|\dot{\tilde{\boldsymbol{q}}}\|^2 + \underline{\lambda}(\boldsymbol{B}_\eta)\|\dot{\boldsymbol{\eta}}\|^2 + \underline{\lambda}(\boldsymbol{K}_P)\|\boldsymbol{\eta}\|^2\right) + U_s(\boldsymbol{\eta} - \tilde{\boldsymbol{q}})$$

$$\beta(\boldsymbol{x}) = \frac{1}{2}\left(\bar{\lambda}(\boldsymbol{M})\|\dot{\tilde{\boldsymbol{q}}}\|^2 + \bar{\lambda}(\boldsymbol{B}_\eta)\|\dot{\boldsymbol{\eta}}\|^2 + \bar{\lambda}(\boldsymbol{K}_P)\|\boldsymbol{\eta}\|^2\right) + U_s(\boldsymbol{\eta} - \tilde{\boldsymbol{q}})$$

and invoking [34, Lemma 4.3], which states that there exist class $\mathcal{K}$ functions a and b such that $a(\|\boldsymbol{x}\|) \leq \alpha(\boldsymbol{x})$ and $b(\|\boldsymbol{x}\|) \geq \beta(\boldsymbol{x})$. In fact, a and b will be of class $\mathcal{K}_\infty$, since α and β are radially unbounded. Note that $\underline{\lambda}(\boldsymbol{B}_\eta) > 0$ was proven in (64).

Proposition 2. *The upper and lower bounds on the Lyapunov function* (74)*, in form of the class K functions a and b, together with the negative semi-definitness of $\dot{V}$, imply that the system* (65)-(66) *is globally, uniformly stable.*

Ad Cond. (ii) of Matrosov's Theorem: In case $\boldsymbol{D}$ is time-invariant, we can simply choose $V^*(\boldsymbol{x}) = \dot{V}(t, \boldsymbol{x})$. Otherwise, we can select

$$V^*(\boldsymbol{x}) = -\bar{\lambda}\left(\boldsymbol{D}(t, \tilde{\boldsymbol{q}}, \boldsymbol{\eta})\right)\|\dot{\tilde{\boldsymbol{q}}}\|^2 - \dot{\boldsymbol{\eta}}^{\mathrm{T}} \boldsymbol{K}_D \dot{\boldsymbol{\eta}}, \tag{76}$$

which satisfies Cond. (ii). We now can deduce the problematic set where $\dot{V}$ becomes zero, namely $E = \{\boldsymbol{x} \in \Omega \ : \ \dot{\tilde{\boldsymbol{q}}} = \dot{\boldsymbol{\eta}} = \boldsymbol{0}\}$.

Ad Cond. (iii) of Matrosov's Theorem: We denote the function $W : [0, \infty) \times \Omega \to \mathbb{R}$ as

$$W(t, \boldsymbol{x}) := \ddot{V}(t, \boldsymbol{x}). \tag{77}$$

To ensure that W satisfies Cond. (iii) we have to establish the boundedness of $|W(t, \boldsymbol{x})|$. From (75) we get

$$W(t, \boldsymbol{x}) = -\Big(2\dot{\tilde{\boldsymbol{q}}}^{\mathrm{T}} \boldsymbol{D} \ddot{\tilde{\boldsymbol{q}}} + \dot{\tilde{\boldsymbol{q}}}^{\mathrm{T}} \dot{\boldsymbol{D}} \dot{\tilde{\boldsymbol{q}}} + 2\dot{\boldsymbol{\eta}}^{\mathrm{T}} \boldsymbol{K}_D \ddot{\boldsymbol{\eta}} + \dot{\boldsymbol{\eta}}^{\mathrm{T}} \dot{\boldsymbol{K}}_D \dot{\boldsymbol{\eta}}\Big). \tag{78}$$

We restrict Ω to be an arbitrarily large, but bounded set. As such, for any starting condition $\boldsymbol{x}(t_0) \in \Omega$, $t_0 \geq 0$, Prop. 2 implies that $\boldsymbol{x}(t)$ is bounded $\forall t \in [t_0, \infty)$. We can conclude directly that all RHS terms of (78), apart from $\ddot{\tilde{\boldsymbol{q}}}$ and $\ddot{\boldsymbol{\eta}}$, are bounded. The boundedness of $\ddot{\tilde{\boldsymbol{q}}}$ and $\ddot{\boldsymbol{\eta}}$ are shown in Sec. B-A.

Ad Cond. (iv) of Matrosov's Theorem: To show that W satisfies condition (iv), we invoke Lemma 1 by B. Paden and R. Panja. The technical details to verify condition (iv.a) are contained in the appendix (see Sec. (B-B)).

To check condition (iv.b) of Lemma 1, we compute the time derivative of W along the solutions of the closed-loop system (65)-(66) and evaluate $\dot{W}$ on the the critical set E

$$\begin{aligned}\dot{W}(t, \boldsymbol{x}) = \ & -2(\boldsymbol{\psi}(\boldsymbol{\eta} - \tilde{\boldsymbol{q}}) + \boldsymbol{K}_P \boldsymbol{\eta})^{\mathrm{T}} \boldsymbol{R}\left(\boldsymbol{\psi}(\boldsymbol{\eta} - \tilde{\boldsymbol{q}}) + \boldsymbol{K}_P \boldsymbol{\eta}\right) \\ & + 2\boldsymbol{\psi}^{\mathrm{T}}(\boldsymbol{\eta} - \tilde{\boldsymbol{q}})^{\mathrm{T}} \boldsymbol{Q}\, \boldsymbol{\psi}(\boldsymbol{\eta} - \tilde{\boldsymbol{q}}), \quad \forall \boldsymbol{x} \in E,\end{aligned} \tag{79}$$

where

$$\begin{aligned}\boldsymbol{Q} &:= \boldsymbol{M}^{-T} \boldsymbol{D} \boldsymbol{M}^{-1} = \boldsymbol{Q}^{\mathrm{T}} \\ \boldsymbol{R} &:= \boldsymbol{B}^{-T} \boldsymbol{K}_D \boldsymbol{B}^{-1} = \boldsymbol{R}^{\mathrm{T}}.\end{aligned}$$

Property 2 implies that $\boldsymbol{M}^{-1}$ is non-singular, $\boldsymbol{D}$ is a real-symmetric, positive definite matrix, hence, Sylvester's Law of Inertia [35] can be applied to show the positive definiteness of $\boldsymbol{Q}$. Similarly, $\boldsymbol{R}$ can be shown to be positive definite. From the positive definiteness of $\boldsymbol{Q}$ and $\boldsymbol{R}$, follows directly that

$\dot{W} \leq \mathbf{0}\ \forall (t, \boldsymbol{x}) \in [t_0, \infty) \times E$, whereby equality hold if and only if $\boldsymbol{x} = \mathbf{0}$. Let us define

$$\boldsymbol{P}(t, \boldsymbol{x}) := \begin{bmatrix} \boldsymbol{Q} + \boldsymbol{R} & \boldsymbol{R}\boldsymbol{K}_P \\ \boldsymbol{K}_P^{\mathrm{T}}\boldsymbol{R} & \boldsymbol{K}_P^{\mathrm{T}}\boldsymbol{R}\boldsymbol{K}_P \end{bmatrix} \in \mathbb{R}^{4n \times 4n},$$

with the following Choleski factorization

$$\begin{bmatrix} \sqrt{\boldsymbol{Q}} & \boldsymbol{R}^{1/2} \\ \mathbf{0} & \boldsymbol{K}_P^{\mathrm{T}}\boldsymbol{R}^{1/2} \end{bmatrix}. \tag{80}$$

From this follows that $\boldsymbol{P}$ is a positive definite matrix which is state- and explicitly time-dependent.[21] This allows us to write the absolute value of $\dot{W}$ in matrix form

$$|\dot{W}(t, \boldsymbol{x})| = 2 \begin{bmatrix} \psi(\boldsymbol{\eta} - \tilde{\boldsymbol{q}}) \\ \boldsymbol{\eta} \end{bmatrix}^{\mathrm{T}} \boldsymbol{P} \begin{bmatrix} \psi(\boldsymbol{\eta} - \tilde{\boldsymbol{q}}) \\ \boldsymbol{\eta} \end{bmatrix}, \quad \forall \boldsymbol{x} \in E. \tag{81}$$

We denote

$$W^*(\boldsymbol{x}) := \underline{P} \left\| \begin{bmatrix} \psi(\boldsymbol{\eta} - \tilde{\boldsymbol{q}}) \\ \boldsymbol{\eta} \end{bmatrix} \right\|^2, \tag{82}$$

where

$$\underline{P} := \inf_{(\boldsymbol{x}, t) \in E \times I} \left\{ \underline{\lambda}(\sqrt{\boldsymbol{Q}}), \underline{\lambda}(\boldsymbol{K}_P) \underline{\lambda} \sqrt{\boldsymbol{R}} \right\} > 0,$$

which allows us to establish the following inequality

$$|\dot{W}(\boldsymbol{x}, t)| \geq W^*(\boldsymbol{x}), \quad \forall \boldsymbol{x} \in E. \tag{83}$$

Clearly, W^* is a time-invariant, positive definite function of $\boldsymbol{x}$. According to [34, Lemma 4.3] there exists a function γ of class $\mathcal{K}_\infty$, such that $W^*(\boldsymbol{x}) \geq \gamma(\|\boldsymbol{x}\|)$. This completes the verification of condition 4(b).

From Prop. 2 we know already that $\boldsymbol{x}$ is bounded. This, together with the continuity of the RHS of (92) and (93) in $\boldsymbol{x}$ and in time through $\boldsymbol{q}_d(t)$ and its time-derivatives we can conclude that the RHS of (92) and (93) are bounded for all $(t, \boldsymbol{x}) \in \mathbb{R}^+ \times \Omega$ for bounded Ω. Moreover, $\boldsymbol{M}$ and $\boldsymbol{B}_\eta$ are bounded (see Prop. 2). Thus, $\boldsymbol{f}$, which is implicitly defined in (92)–(93), is bounded on $\mathbb{R}^+ \times \Omega$ for bounded Ω and the last condition of Matrosov's Theorem is fulfilled.

So far all conditions of Matrosov's Theorem have been shown to be satisfied. In addition we can use the first inequality of Cond. (i) to determine the region of attraction. For any initial condition $\boldsymbol{x}_0 \in \mathbb{R}^{4n}$ we can find an appropriate α and Ω via Cond. (i) such that $\boldsymbol{x}_0$ is element of $V_{t,\alpha}^{-1}$. Thus, according to Matrosov's Theorem, the origin $[\tilde{\boldsymbol{q}}, \boldsymbol{\eta}, \dot{\tilde{\boldsymbol{q}}}, \dot{\boldsymbol{\eta}}]^{\mathrm{T}} = \mathbf{0}$ is an uniformly globally asymptotically stable equilibrium point of the closed-loop system (65)–(66). ∎

VII. Experimental Validation and Performance Analysis

The performance of the control approaches have been experimentally evaluated on the first five variable stiffness actuators (VSA) joints of the DLR Hand Arm System [1], see also Fig. 1. The first four arm joints, namely the elbow and the three shoulder joints, are implemented by Floating Spring Joints (FSJ) [2]. The under arm rotation is realized via a bidirectional antagonistic variable stiffness (BAVS) joint [3]. Here we want to emphasize that the ESP control concept is not limited to one class of VSA joints but works on any type that fulfills the conditions in Sec. II.

First, we introduce an approach to design the damping matrix $\boldsymbol{D}$. For the design of the matrix it should be mentioned that the proposed control concept allows for any damping matrix that satisfies Assumption 4. However, for the experiments presented in this paper we apply the approach presented below which has proven to work well in practice. In the latter part, Sec. VII-B, we present the experimental results.

A. Damping Design

As the inertia of the robot system is configuration dependent, it varies significantly throughout its workspace. In addition the stiffness of each joint strongly depends on the load. As the robot moves through its workspace, the gravitational and dynamical load change constantly and so do the joints stiffness's. External forces may additionally affect the stiffness's of the joints. As we aim for similar performance throughout the entire workspace of the robot, we apply a damping design that takes these effects into account. The design of the link-side damping matrix $\boldsymbol{D}$ as well as the controller gain $\boldsymbol{K}_D$ are based on modal decomposition.

For the damping design we consider the variation of $\boldsymbol{M}(\boldsymbol{q})$ to be slow such that its derivative can be neglected. In addition, we approximate the joint torque $\psi(\boldsymbol{\eta} - \tilde{\boldsymbol{q}})$ by the local stiffness $\boldsymbol{\kappa}(\boldsymbol{\eta} - \tilde{\boldsymbol{q}})$ times the virtual joint deflection $\boldsymbol{\eta} - \tilde{\boldsymbol{q}}$. As a result, the link-side closed-loop dynamics (37) reduces to

$$\boldsymbol{M}(\boldsymbol{q})\ddot{\tilde{\boldsymbol{q}}} + \boldsymbol{D}(\boldsymbol{\eta}, \tilde{\boldsymbol{q}})\dot{\tilde{\boldsymbol{q}}} - \boldsymbol{\kappa}(\boldsymbol{\eta} - \tilde{\boldsymbol{q}})(\boldsymbol{\eta} - \tilde{\boldsymbol{q}}) = 0. \tag{84}$$

Since $\boldsymbol{M}$ is positive definite and $\boldsymbol{\kappa}$ symmetric we can simultaneously diagonalize these two matrices by a non-singular matrix $\boldsymbol{Q} \in \mathbb{R}^{n \times n}$, such that $\boldsymbol{Q}^{\mathrm{T}}\boldsymbol{Q} = \boldsymbol{M}$ and $\boldsymbol{Q}^{\mathrm{T}}\boldsymbol{\Lambda}\boldsymbol{Q}$. Matrix $\boldsymbol{\Lambda}(\boldsymbol{\eta}, \tilde{\boldsymbol{q}})$ is diagonal with the positive generalized eigenvalues of $\boldsymbol{\kappa}$ with respect to $\boldsymbol{M}$ as its elements. This allows us to rewrite (84) as

$$\begin{aligned} &\boldsymbol{Q}^{\mathrm{T}}(t, \boldsymbol{\eta}, \tilde{\boldsymbol{q}})\boldsymbol{Q}(t, \boldsymbol{\eta}, \tilde{\boldsymbol{q}})\ddot{\tilde{\boldsymbol{q}}} + \boldsymbol{D}(t, \boldsymbol{\eta}, \tilde{\boldsymbol{q}}) \\ &- \boldsymbol{Q}^{\mathrm{T}}(t, \boldsymbol{\eta}, \tilde{\boldsymbol{q}})^{\mathrm{T}}\boldsymbol{\Lambda}\boldsymbol{Q}(t, \boldsymbol{\eta}, \tilde{\boldsymbol{q}}) = \mathbf{0} \end{aligned}$$

By choosing the damping matrix as

$$\boldsymbol{D} = 2\boldsymbol{Q}^{\mathrm{T}}(t, \boldsymbol{\eta}, \tilde{\boldsymbol{q}})\boldsymbol{D}_\xi \boldsymbol{\Lambda}^{1/2}(\boldsymbol{\eta}, \tilde{\boldsymbol{q}})\boldsymbol{Q}(t, \boldsymbol{\eta}, \tilde{\boldsymbol{q}}), \tag{85}$$

where $\boldsymbol{D}_{\xi_D}$ is a diagonal matrix with the modal damping factors $\xi_{D,i} \in [0, 1]$ as elements. We now introduce new coordinates $\boldsymbol{z} = \boldsymbol{Q}(t, \boldsymbol{\eta}, \tilde{\boldsymbol{q}})\tilde{\boldsymbol{q}}$ in order to obtain a system of n decoupled equations

$$\ddot{\boldsymbol{z}} + 2\boldsymbol{D}_{\xi_D}\boldsymbol{\Lambda}^{1/2}\dot{\boldsymbol{z}} + \boldsymbol{\Lambda}\boldsymbol{z} = \mathbf{0}, \tag{86}$$

where the effects of the damping parameters $\boldsymbol{\xi}_{D,i}$ become clear. For the design of $\boldsymbol{K}_D$ we consider the system

$$\boldsymbol{M}_{\boldsymbol{\eta}}(t, \boldsymbol{\eta}, \tilde{\boldsymbol{q}}, \dot{\tilde{\boldsymbol{q}}})\ddot{\boldsymbol{\eta}} + \boldsymbol{K}_D\dot{\boldsymbol{\eta}} + \boldsymbol{\kappa}(\boldsymbol{\eta} - \tilde{\boldsymbol{q}})(\boldsymbol{\eta} - \tilde{\boldsymbol{q}}) + \boldsymbol{K}_P\boldsymbol{\eta} \tag{87}$$

and proceed analogously to above – resulting in a time and state-dependent damping matrix $\boldsymbol{K}_D$.

Remark 4. This damping design implies the matrix $\boldsymbol{D}(t, \boldsymbol{\eta}, \boldsymbol{q})$ to be a function of the link error-variables $\tilde{\boldsymbol{q}}$ and motor variables $\boldsymbol{\eta}$ and an explicit function of time t. As a consequence, in order to calculate $\dot{\boldsymbol{D}}$ and $\ddot{\boldsymbol{D}}$ we require the first

[21] For real-symmetric matrices $\boldsymbol{P}$, the following statements are equivalent: (1) $\boldsymbol{P}$ is positive definite and (2) $\boldsymbol{P} = \boldsymbol{B}\boldsymbol{B}^{\mathrm{T}}$ for some non-singular $\boldsymbol{B}$ [36].

and second time derivatives of the generalized eigenvalues and eigenvectors. The interested reader can find more details about this issue in [37] and [38].

Remark 5. Simulations and experiments for the DLR Hand Arm System have shown, that neglecting all terms that contain $\dot{\boldsymbol{D}}$ and $\ddot{\boldsymbol{D}}$, in the implementation of the control law, has no significant impact on the control performance. With this in mind and in order to reduce the computational load we neglect these terms for the practical implementation.

B. Experimental Results

Throughout all experiments the controller parameters were kept constant and set as follows: $\boldsymbol{K}_P = \text{diag}(1000, 900, 750, 750, 750)$, $\xi_{D,i} = 0.5$, $\xi_{K_D,i} = 0.7$, $i = 1, \ldots, 5$. $\boldsymbol{K}_P$ was manually set such that for the medium stiffness setting none of the control inputs overshoot the maximal motor torques of 65 Nm for the FSJ joints and 4 Nm for the BAVS joint, respectively.

Remark 6. In standard operational mode, saturation of the control input never has caused any issues so far. Nevertheless, to allow a fair performance analysis, the gains were set such that saturation effects are avoided for the majority of experiments.

We performed three different experiments. No friction compensation was active throughout the experiments. Thus, viscous friction affects the transient tracking performance and static friction leads to non-zero steady-state errors. For low stiffness values, friction effects such as stiction have a crucial impact on the steady-state errors. Sensor uncertainties for motor and link angles lead to uncertain spring torques and gravity torques calculations, which again increase the steady-state errors. Bear in mind, that due to some technical sensor issues on the second joint the control input for the second joint is significantly more noisy, compared to the other four joints.

The first experiment shows the disturbance rejection and damping performances of an ESP and ESP+ controller. They are compared to the well-known motor PD controller by Tomei [4]. The setup was as follows: a 3 kg mass that swings on a rope impacts,in a reproducible manner, with the robot, see Fig. 11.[22] The robot is commanded to keep its pre-impact position. This experiment has been performed for all three controllers for three different stiffness settings: minimum ($\sigma = 0°$), medium ($\sigma = 5°$) and maximum ($\sigma = 10°$) stiffness, which correspond to the outer, middle and inner curves of Fig. 1(b–c), respectively. The results are shown in Fig. 12. The convergence rate increases with decreasing joint stiffness settings. This behavior is as expected, as our control concepts preserve the intrinsic joint elasticities. Hence, the intrinsic stiffness values of the physical joints act as PD gains on the link positions. The differences in convergence rates are less than one might expect. This is due to nonlinear nature of the elasticities, the local stiffness depends on the joint deflection and thereby on the external load, cf. Fig. 13. As a result, joint 4, which faces the highest external load, reaches relatively high maximum local stiffness values for all experiments. To emphasize the elasticity

[22]Below you can find the link to a video that shows this experiment.

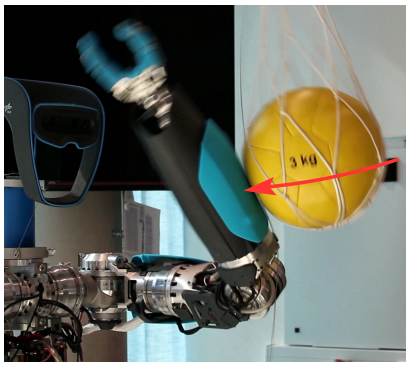

Fig. 11. This photo shows the impact experiment setup, the red arrow indicates the trajectory of ball. The shot was taken during the impact phase.

and oscillatory behavior of the robot system, and the need for elaborate damping control concepts, the performance of a simple motor PD controller (Tomei [4]) is shown as reference. As shown in Fig. 12 its damping performance is very limited. For the soft stiffness setting the control inputs of the ESP and ESP+ controller are heavily saturated for an extended amount of time. Despite these saturations, the stability of the system is not impaired at all. Furthermore, both control approaches show impressive damping and disturbance rejection performances with hardly any overshooting in presence of these saturations. This is one of the impressive features of ESP and ESP+ control. We did not adapt the controller gains in order to show how the controllers perform over a vast joint stiffness range (approx. one order of magnitude variation) with equal gains. In that regard, the ESP turns out to be superior as the control signals are significantly less noisy for the soft stiffness setting, while achieving comparable performance. For the medium stiffness setting, for which the controllers have been manually tuned, ESP+ control proves to be superior. The control input amplitude is significantly lower compared to the ESP controller. In addition, the ESP+ controller basically does not overshoot at all. We can conclude, despite the fact that the joint stiffness values vary in the range of approx. one order of magnitude the ESP and ESP+ controllers perform excellent without adapting the gains.

The second experiment highlights the tracking performance. The results are contained in Fig. 14. The joints reach maximum angular velocities of $\dot{\boldsymbol{q}}_{max}^{\mathrm{T}} = [\ 218\ 79\ 117\ 128\ 329\ ]$ deg/s. Friction as well as model and sensor uncertainties are sources of the non-zero steady-state error.

The third experiment shows the disturbance rejection and damping performance while the robot moves along a trajectory. An external disturbance is applied through physical interaction with a human. The magnitude of disturbance correlates with the peaks in the corresponding joint torque plots in Fig. 15. Even while the robot is in motion the ESP and ESP+ controllers show impressive disturbance rejection performance. Within approximately 0.3 seconds the disturbances are rejected and the robot returns on its desired trajectory. The ESP+ controller shows slightly less overshooting as can be seen graphs of the tracking error $\tilde{\boldsymbol{q}}$.

Below we give direct links to three videos that demonstrate the performance of the ESP and ESP+ control approaches on

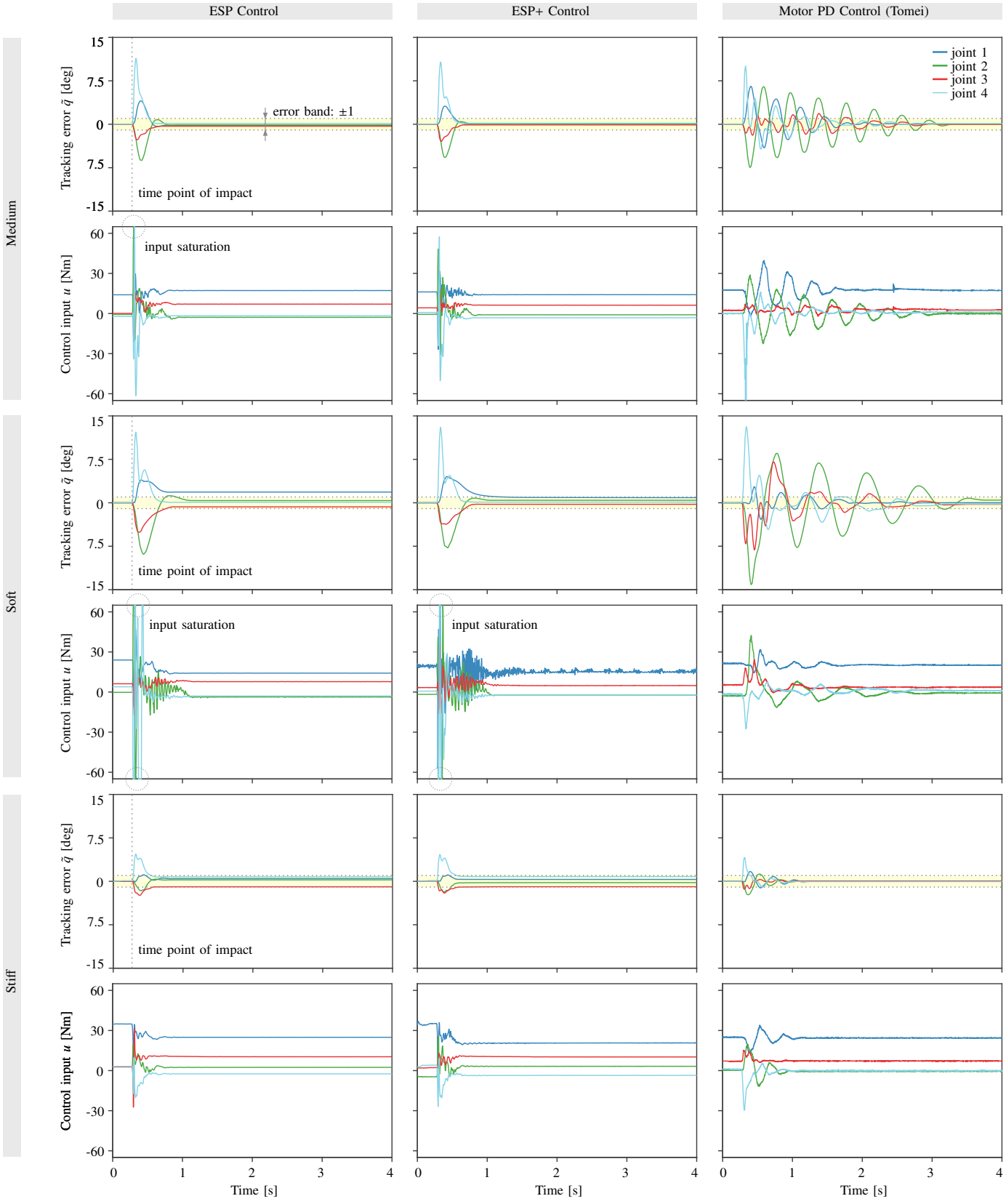

Fig. 12. The plots show the results of the impact experiment. The DLR Hand Arm System is hit, in a reproducible manner, on the under arm with a mass of 3 kg that swings on a rope. The damping performances of the ESP controller (left column), ESP+ controller (center column) and the well known motor PD controller by Tomei [4] (right column) are shown in comparison. Throughout the experiment the robot is commanded to hold its link configuration. The experiment is performed for three different stiffness settings (soft, medium and stiff). Under ESP and ESP+ control, on the middle stiffness setting, the links tracking errors $\tilde{\boldsymbol{q}}$ converge withing 0.25 s post impact into an ±1 deg error band.

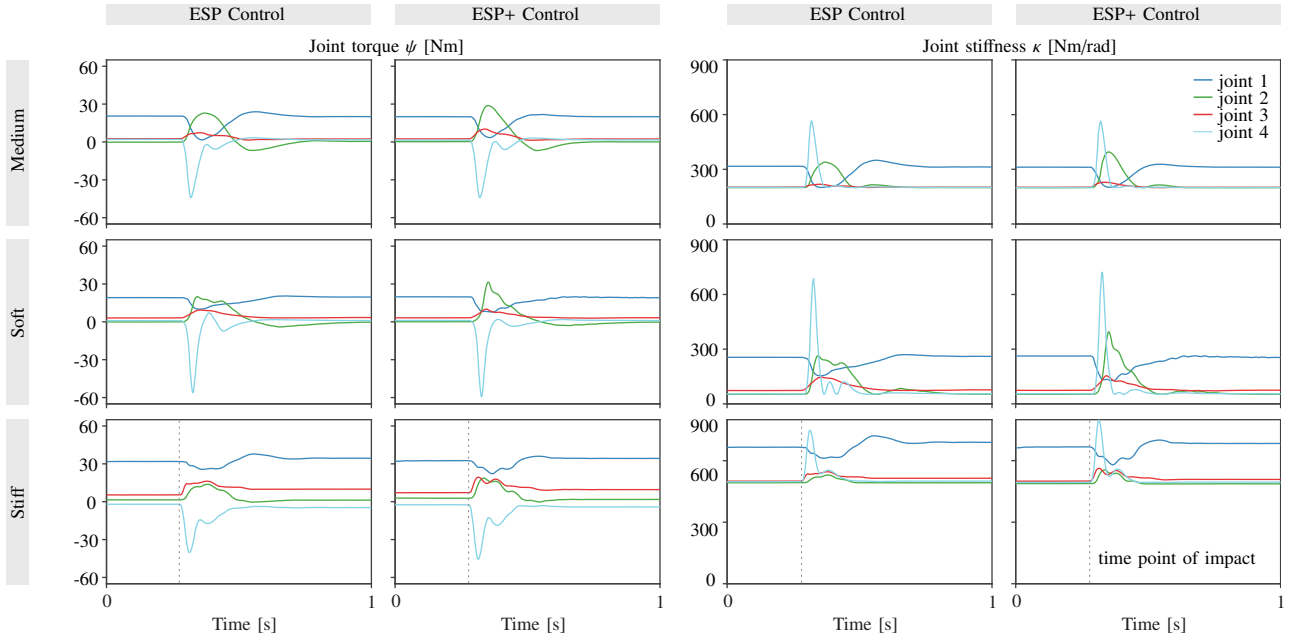

Fig. 13. Continuation of the impact experiment results. Due to the nature of the nonlinear elasticities the local stiffness values change continuously throughout the course of each experiment as they are dependent on the spring deflection and as such increase with increasing joint loads (cf. 1 b).

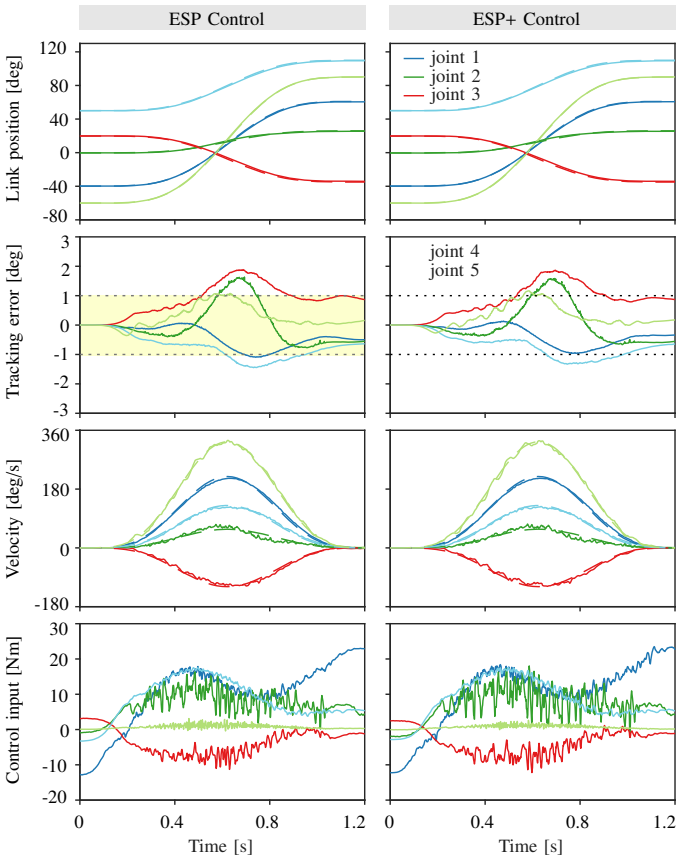

Fig. 14. Tracking performance in absence of external disturbances.

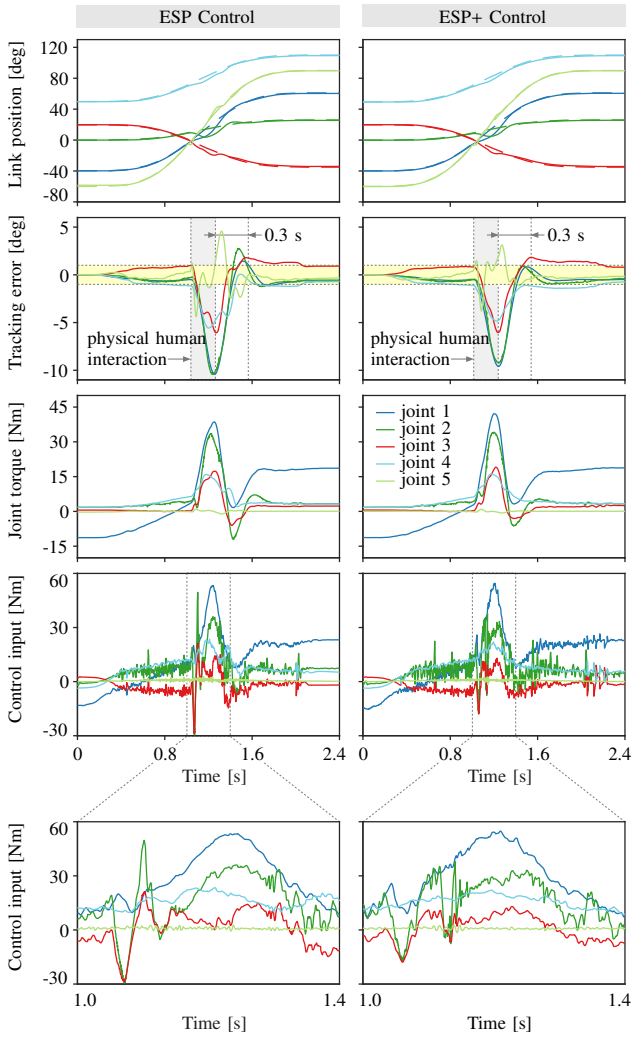

Fig. 15. The system is externally disturbed by physical human interaction while following a reference trajectory.

the DLR Hand Arm Sytem.

- ESP control showcase video:
  http://rmc.dlr.de/rm/de/staff/extcms/images/rmc/2016_ICRA_Keppler.mp4
- ESP+ control showcase video: among other things, the ball impact experiment presented above is shown.
  https://www.youtube.com/watch?v=PATvv47QfQs
- The following video shows the DLR Hand Arm System drill hammering into concrete. This task requires both, precise positioning of the tool center point and vibration damping. The performance is enabled by ESP control.
  https://www.youtube.com/watch?v=JVdufPRK4NI

Remark 7. ESP control allows to compensate virtual or physical joint-space forces that are due to a C^2 potential field. This allows for several interesting applications, e.g. it can be exploited to enable compliant robots to interact with the environment in a desired manner.

VIII. Conclusion

The ESP control approach presented in this paper yields a globally stable, link-side tracking controller that allows simultaneous link-side damping assignment for compliantly actuated robots with nonlinear elastic transmissions. The control framework incorporates, at a fundamental level, the system's inherent physical structure and aims to minimize the dynamic shaping. This manifests itself in the preservation of the elastic structure of the original system, i.e., the link of the closed-loop system remains connected to the motor via the original elastic element. Therefore we coin the name 'Elastic Structure Preserving' (ESP) Control. As such, the stiffness of the real physical spring acts as proportional gain to drive the link to its desired position. ESP Control focuses on preserving the motor-side inertial properties while the ESP+ approach aims at minimizing the dynamic shaping on the motor side. On the basis of a theoretical analysis for a single joint, we showed that our approach changes the plant dynamics significantly less than feedback linearization-based FSF control.

The physically motivated nature of the design approach provides several benefits. The resulting closed-loop dynamics can be represented by a multi-spring damper system. This provides us with a physically intuitive interpretation of the controller. In particular, it proves highly valuable for the tuning stage as the gains can be interpreted as springs and dampers, respectively.

The controller concept imposes neither lower nor upper bounds on the controller gains. In addition, it allows the damping on the motor and on the link side to be state-dependent. The transition to the rigid robot case, i.e., when the stiffness values of each joint approach infinity, yields the well-known PD+ controller [27] and thus no high-gain design.

The approach has been extensively experimentally evaluated on a multi-joint VSA robot arm. It shows impressive performance and robustness against external disturbances. It also appears to be quiet robust against input saturations. As for any link-side tracking controller, a theoretical limitation of the approach seemed to be the usage of the second and third time derivative of the measured link position in the control law, which however turned out not to be a practical limitation, since the time derivatives could be computed based on an accurate model of the plant. We plan to investigate if the proposed control concepts can be generalized to a more general class of elastic robots in which Assumptions 1 and 2 can be relaxed.

To our best knowledge, this is the first link-side tracking controller for compliantly actuated robots with nonlinear elastic transmissions, which is theoretically founded and reported to be experimentally validated on a multi-degrees of freedom robot.

Appendix A
Function definitions and a Lemma by Merikoski

Applying (38) we can rewrite $\boldsymbol{\kappa}(\boldsymbol{\theta}-\boldsymbol{q})$ in new coordinates

$$\boldsymbol{\kappa}(\boldsymbol{\theta}-\boldsymbol{q}) = \boldsymbol{\kappa}\Big(\boldsymbol{\psi}^{-1}(\boldsymbol{\psi}(\boldsymbol{\eta}-\tilde{\boldsymbol{q}}) + \boldsymbol{n}(t,\tilde{\boldsymbol{q}},\dot{\tilde{\boldsymbol{q}}}))\Big) =: \boldsymbol{\chi}(t,\boldsymbol{\eta},\tilde{\boldsymbol{q}},\dot{\tilde{\boldsymbol{q}}}). \quad (88)$$

Equation (88), together with (41), allows us to define $\boldsymbol{A}$ as

$$\boldsymbol{A}(t,\boldsymbol{\eta},\tilde{\boldsymbol{q}},\dot{\tilde{\boldsymbol{q}}}) := \boldsymbol{\chi}^{-1}(t,\boldsymbol{\eta},\tilde{\boldsymbol{q}},\dot{\tilde{\boldsymbol{q}}})\boldsymbol{\kappa}(\boldsymbol{\eta}-\tilde{\boldsymbol{q}}). \quad (89)$$

Equations (38), (42) and (88) yield $\boldsymbol{a}$ as follows

$$\boldsymbol{a}(t,\boldsymbol{\eta},\tilde{\boldsymbol{q}},\dot{\tilde{\boldsymbol{q}}},\ddot{\tilde{\boldsymbol{q}}}) := \tilde{\boldsymbol{q}} + \boldsymbol{q}_d(t) + \boldsymbol{\chi}^{-1}(t,\boldsymbol{\eta},\tilde{\boldsymbol{q}},\dot{\tilde{\boldsymbol{q}}})\boldsymbol{\gamma}(t,\boldsymbol{\eta},\tilde{\boldsymbol{q}},\dot{\tilde{\boldsymbol{q}}},\ddot{\tilde{\boldsymbol{q}}}). \quad (90)$$

Lemma 2 (J. K. Merikoski and R. Kumar, [39])**.** *If $\boldsymbol{A}$ and $\boldsymbol{B}$ are Hermitian and non-negative definite, then we can both underestimate and overestimate eigenvalues of $\boldsymbol{AB}$ by using eigenvalues of $\boldsymbol{A}$ and $\boldsymbol{B}$.*

$$\lambda_i(\boldsymbol{A})\lambda_{min}(\boldsymbol{B}) \le \lambda_i(\boldsymbol{AB}) \le \lambda_i(\boldsymbol{A})\lambda_{max}(\boldsymbol{B}). \quad (91)$$

Appendix B
Boundedness and continuity of some functions

A. Ad Condition (iii) of Matrosov's Theorem

In Sec. VI we have already established the boundedness of $\boldsymbol{x}$. This, together with Ass. 3, implies that $\boldsymbol{q}$ and $\dot{\boldsymbol{q}}$ are bounded as well. As $\boldsymbol{M} \in C^2$ and $\boldsymbol{q}$ is bounded, the tensors $\frac{\partial \boldsymbol{M}(\boldsymbol{q})}{\partial \boldsymbol{q}}$ and $\frac{\partial^2 \boldsymbol{M}(\boldsymbol{q})}{\partial \boldsymbol{q}^2}$ are bounded. We can conclude that $\dot{\boldsymbol{M}}(\boldsymbol{q})$ is bounded. Due to Prop. 2, $\boldsymbol{M}^{-1}$ exists and is bounded. This, together with the fact that all terms on the RHS of the closed-loop link dynamics

$$\boldsymbol{M}(t,\tilde{\boldsymbol{q}})\ddot{\tilde{\boldsymbol{q}}} = -\Big(\boldsymbol{C}(t,\tilde{\boldsymbol{q}},\dot{\tilde{\boldsymbol{q}}}) - \boldsymbol{D}(t,\tilde{\boldsymbol{q}},\boldsymbol{x})\Big)\dot{\tilde{\boldsymbol{q}}} + \boldsymbol{\psi}(t,\boldsymbol{x}-\tilde{\boldsymbol{q}}), \quad (92)$$

are bounded, implies that $\ddot{\tilde{\boldsymbol{q}}}$ is bounded.[23] Boundedness of $\ddot{\boldsymbol{q}}$ results from Ass. 3. This again, implies that $\ddot{\boldsymbol{M}}(\boldsymbol{q})$ is bounded.[24] Further, $\ddot{\tilde{\boldsymbol{q}}}$ is continuous in $\tilde{\boldsymbol{q}}, \dot{\tilde{\boldsymbol{q}}}, \boldsymbol{\eta}$ and in t through the bounded functions $\boldsymbol{q}_d(t)$ and $\dot{\boldsymbol{q}}_d(t)$.

The reasoning for the boundedness of $\ddot{\boldsymbol{\eta}}$ goes along the same lines as for $\ddot{\tilde{\boldsymbol{q}}}$. For (66) we can write

$$\boldsymbol{B}_\eta(t,)\ddot{\boldsymbol{\eta}} = -\boldsymbol{C}_\eta(t,)\dot{\boldsymbol{\eta}} - \boldsymbol{\psi}(\boldsymbol{\eta}-\tilde{\boldsymbol{q}}) - \boldsymbol{K}_P\boldsymbol{\eta} - \boldsymbol{K}_D\dot{\boldsymbol{\eta}} \quad (93)$$

From the analysis so far, we can directly conclude the boundedness of the last three terms. We can upper bound the norm[25] of $\boldsymbol{C}_\eta$

$$\|\boldsymbol{C}_\eta\| \le \|\boldsymbol{A}\|\,\|\boldsymbol{B}\|\,\|\dot{\boldsymbol{A}}\|. \quad (94)$$

[23] Note, $\|\boldsymbol{C}(\boldsymbol{q},\dot{\boldsymbol{q}})\| \le k_C\|\dot{\boldsymbol{q}}\|$, for some positive constant k_C.
[24] Which is equivalent to the statement that $\dot{\boldsymbol{C}}$ is bounded.
[25] Any matrix norm can be used here.

We now analyze each of the RHS terms. Considering Ass. 1, the continuity of $\boldsymbol{\kappa}$ in its arguments, the continuity of $\boldsymbol{\chi}$ in the states and continuity in the time, through the bounded functions $\boldsymbol{q}_d(t), \dot{\boldsymbol{q}}_d(t)$, and the boundedness of $\boldsymbol{x}$, we know that $\boldsymbol{A}$ is bounded and continuous in time through bounded functions. $\boldsymbol{B}$ is bounded by model assumptions. For $\dot{\boldsymbol{A}}$ we can write

$$\dot{\boldsymbol{A}} = \dot{\boldsymbol{\chi}}^{-1}(t, \tilde{\boldsymbol{q}}, \dot{\tilde{\boldsymbol{q}}})\boldsymbol{\kappa}(\boldsymbol{\eta} - \tilde{\boldsymbol{q}}) + \boldsymbol{\chi}^{-1}(t, \tilde{\boldsymbol{q}}, \dot{\tilde{\boldsymbol{q}}})\dot{\boldsymbol{\kappa}}(\boldsymbol{\eta} - \tilde{\boldsymbol{q}}) \tag{95}$$

where $\dot{\boldsymbol{\chi}}^{-1}(t, \tilde{\boldsymbol{q}}, \dot{\tilde{\boldsymbol{q}}}) = -\boldsymbol{\chi}^{-1}(t, \tilde{\boldsymbol{q}}, \dot{\tilde{\boldsymbol{q}}})\dot{\boldsymbol{\chi}}(t, \tilde{\boldsymbol{q}}, \dot{\tilde{\boldsymbol{q}}})\boldsymbol{\chi}^{-1}(t, \tilde{\boldsymbol{q}}, \dot{\tilde{\boldsymbol{q}}})$. Due to Ass. 1, the inverse of $\boldsymbol{\chi}$ exists, is bounded and continuous in the states and time through bounded functions $\boldsymbol{q}_d(t), \dot{\boldsymbol{q}}_d(t)$. Exploiting Ass. 1, we can argue that $\dot{\boldsymbol{\chi}}(t, \tilde{\boldsymbol{q}}, \dot{\tilde{\boldsymbol{q}}})$ is continuous in the states $\boldsymbol{x}$, in $\ddot{\tilde{\boldsymbol{q}}}$ and in time, through bounded functions $\boldsymbol{q}_d(t), \dot{\boldsymbol{q}}_d(t), \ddot{\boldsymbol{q}}_d(t)$. Considering also the boundedness of $\boldsymbol{x}, \ddot{\tilde{\boldsymbol{q}}}, \ddot{\boldsymbol{q}}_d(t)$ we can conclude the boundedness of$\dot{\boldsymbol{\chi}}(t, \tilde{\boldsymbol{q}}, \dot{\tilde{\boldsymbol{q}}})$. Analogous statements can be derived for $\boldsymbol{\kappa}(\boldsymbol{\eta}-\tilde{\boldsymbol{q}})$ and $\dot{\boldsymbol{\kappa}}(\boldsymbol{\eta}-\tilde{\boldsymbol{q}})$. In the end we can conclude that $\boldsymbol{C}_\eta$ is continuous in $\boldsymbol{x}$, $\ddot{\tilde{\boldsymbol{q}}}$ and t and depends on time through bounded functions $\boldsymbol{q}_d(t), \dot{\boldsymbol{q}}_d(t), \ddot{\boldsymbol{q}}_d(t)$.

From (64) we know that the inverse of $\boldsymbol{B}_\eta$ exists and that it is bounded. Which leads us to the conclusion, that $\ddot{\boldsymbol{\eta}}$ is bounded, continuous in the states $\boldsymbol{x}$, in $\ddot{\tilde{\boldsymbol{q}}}$ and in time t through the bounded functions $\boldsymbol{q}_d(t), \dot{\boldsymbol{q}}_d(t), \ddot{\boldsymbol{q}}_d(t)$.

B. Verification of Condition (iv.a) of Lemma 1

In Sec. B-A we have established that $\ddot{\tilde{\boldsymbol{q}}}, \ddot{\boldsymbol{\eta}}$ are continuously in the tracking errors $\boldsymbol{x}$ and depend continuously on time through $\boldsymbol{q}_d(t), \dot{\boldsymbol{q}}_d(t), \ddot{\boldsymbol{q}}_d(t)$, which are bounded. To verify that $\dot{W}$ satisfies condition (iv.a) of Paden and Panja's lemma, we have yet to show that $\tilde{\boldsymbol{q}}^{(3)}, \boldsymbol{\eta}^{(3)}$ are continuously in the tracking errors $\boldsymbol{x}$ and depend continuously on time through a bounded function.

To show that $\tilde{\boldsymbol{q}}^{(3)}$ is bounded we differentiate (65) with respect to time and rearrange some terms

$$\begin{aligned}\boldsymbol{M}(t, \tilde{\boldsymbol{q}})\frac{\mathrm{d}}{\mathrm{dt}}\left(\ddot{\tilde{\boldsymbol{q}}}\right) &= -\dot{\boldsymbol{M}}(t, \tilde{\boldsymbol{q}})\ddot{\tilde{\boldsymbol{q}}} - \boldsymbol{C}(t, \tilde{\boldsymbol{q}}, \dot{\tilde{\boldsymbol{q}}})\ddot{\tilde{\boldsymbol{q}}} - \dot{\boldsymbol{C}}(t, \tilde{\boldsymbol{q}}, \dot{\tilde{\boldsymbol{q}}})\dot{\tilde{\boldsymbol{q}}} \\ &- \boldsymbol{D}(t, \tilde{\boldsymbol{q}}, \boldsymbol{x})\ddot{\tilde{\boldsymbol{q}}} - \dot{\boldsymbol{D}}(t, \tilde{\boldsymbol{q}}, \boldsymbol{x})\dot{\tilde{\boldsymbol{q}}} + \boldsymbol{\kappa}(\boldsymbol{\eta} - \tilde{\boldsymbol{q}})(\dot{\boldsymbol{\eta}} - \dot{\tilde{\boldsymbol{q}}}).\end{aligned} \tag{96}$$

All RHS terms have been shown to be bounded, continuous with respect to the tracking error and depend continuously on time through bounded functions.[26] As $\boldsymbol{M}^{-1}$ is bounded, we can conclude that $\tilde{\boldsymbol{q}}^{(3)}$ exists and depends continuously on the tracking error and continuously on time through bounded functions $\boldsymbol{q}_d(t), \dot{\boldsymbol{q}}_d(t), \ddot{\boldsymbol{q}}_d(t)$.

For $\boldsymbol{\eta}^{(3)}$ we can proceed in analog fashion. We differentiate (66) with respect to time and rearrange some terms

$$\begin{aligned}\boldsymbol{B}_\eta(t, \tilde{\boldsymbol{q}})\frac{\mathrm{d}}{\mathrm{dt}}(\ddot{\boldsymbol{\eta}}) &= -\dot{\boldsymbol{B}}_\eta(t, \tilde{\boldsymbol{q}})\ddot{\boldsymbol{\eta}} - \boldsymbol{C}_\eta(t, \tilde{\boldsymbol{q}}, \dot{\tilde{\boldsymbol{q}}})\ddot{\boldsymbol{\eta}} - \dot{\boldsymbol{C}}_\eta(t, \tilde{\boldsymbol{q}}, \dot{\tilde{\boldsymbol{q}}})\dot{\boldsymbol{\eta}} \\ &- \boldsymbol{\kappa}(\boldsymbol{\eta} - \tilde{\boldsymbol{q}})(\dot{\boldsymbol{\eta}} - \dot{\tilde{\boldsymbol{q}}}) - \boldsymbol{K}_D\ddot{\boldsymbol{\eta}} - \boldsymbol{K}_P\dot{\boldsymbol{\eta}}.\end{aligned} \tag{97}$$

The only terms we still have to analyze are $\dot{\boldsymbol{B}}_\eta$ and $\dot{\boldsymbol{C}}_\eta$. We can apply the results from Sec. B-A to argue that $\dot{\boldsymbol{B}}_\eta = 2\boldsymbol{A}^{\mathrm{T}}\boldsymbol{B}\dot{\boldsymbol{A}}$ is continuous in the states $\boldsymbol{x}$, $\dot{\tilde{\boldsymbol{q}}}$ and in time through bounded functions $\boldsymbol{q}_d(t), \ddot{\boldsymbol{q}}_d(t), \ddot{\boldsymbol{q}}_d(t)$. To give an analog statement for $\dot{\boldsymbol{C}}_\eta = \dot{\boldsymbol{A}}^{\mathrm{T}}\boldsymbol{B}\dot{\boldsymbol{A}} + \boldsymbol{A}^{\mathrm{T}}\boldsymbol{B}\ddot{\boldsymbol{A}}$ we have yet to analyze $\ddot{\boldsymbol{A}}$. The straight-forward, but tedious computations, we used to analyze $\dot{\boldsymbol{A}}$ can be extended to show that $\ddot{\boldsymbol{A}}$ is a continuous function in $\boldsymbol{x}$, $\ddot{\tilde{\boldsymbol{q}}}, \tilde{\boldsymbol{q}}^{(3)}$ and in time through bounded functions $\boldsymbol{q}_d(t), \ldots, \boldsymbol{q}_d^{(3)}(t)$. To do so, one only has to the take the continuity and boundness properties of $\tilde{\boldsymbol{q}}^{(3)}$ that we have shown above and the fact that $U_s \in C^4$ additionally into consideration.

[26] See Sec. VI and Sec. B-A.

References

[1] A. Albu-Schäffer, O. Eiberger, M. Fuchs, M. Grebenstein, S. Haddadin, C. Ott, A. Stemmer, T. Wimböck, S. Wolf, C. Borst, and G. Hirzinger, "Anthropomorphic soft robotics – from torque control to variable intrinsic compliance," in *Robotics Research*, ser. Springer Tracts in Advanced Robotics, C. Pradalier, R. Siegwart, and G. Hirzinger, Eds. Springer, 2011, vol. 70, pp. 185–207.

[2] S. Wolf, O. Eiberger, and G. Hirzinger, "The dlr fsj: Energy based design of a variable stiffness joint," in *Robotics and Automation (ICRA), 2011 IEEE International Conference on*, May 2011, pp. 5082–5089.

[3] W. Friedl, H. Höppner, F. Petit, and G. Hirzinger, "Wrist and forearm rotation of the dlr hand arm system: Mechanical design, shape analysis and experimental validation," in *Intelligent Robots and Systems (IROS), 2011 IEEE/RSJ International Conference on*. IEEE, 2011, pp. 1836–1842.

[4] P. Tomei, "A simple pd controller for robots with elastic joints," *Automatic Control, IEEE Transactions on*, vol. 36, no. 10, pp. 1208–1213, Oct 1991.

[5] R. Ortega, R. Kelly, and A. Loria, "A class of output feedback globally stabilizing controllers for flexible joints robots," *Robotics and Automation, IEEE Transactions on*, vol. 11, no. 5, pp. 766–770, Oct 1995.

[6] L. Zollo, A. De Luca, and B. Siciliano, "Regulation with on-line gravity compensation for robots with elastic joints," in *Robotics and Automation, 2004. Proceedings. ICRA '04. 2004 IEEE International Conference on*, vol. 3, April 2004, pp. 2687–2692.

[7] C. Ott, A. Albu-Schäffer, A. Kugi, S. Stamigioli, and G. Hirzinger, "A passivity based cartesian impedance controller for flexible joint robots-part i: Torque feedback and gravity compensation," in *Proc. IEEE Int. Conf. on Robotics and Automation*, 2004.

[8] B. Vanderborght, A. Albu-Schäffer, A. Bicchi, E. Burdet, D. G. Caldwell, R. Carloni, M. Catalano, O. Eiberger, W. Friedl, G. Ganesh *et al.*, "Variable impedance actuators: A review," *Robotics and Autonomous Systems*, vol. 61, no. 12, pp. 1601–1614, 2013.

[9] A. Albu-Schäffer, C. Ott, and F. Petit, "Constructive energy shaping control for a class of euler-lagrange systems," in *10th Int. IFAC Symposium on Robot Control*, 2012.

[10] A. Albu-Schäffer and G. Hirzinger, "A globally stable state feedback controller for flexible joint robots," *Advanced Robotics*, vol. 15, no. 8, pp. 799–814, 2001.

[11] F. Petit and A. Albu-Schäffer, "State feedback damping control for a multi dof variable stiffness robot arm," in *Proc. IEEE Int. Conf. on Robotic and Automation*, 2011.

[12] I. Sardellitti, G. Medrano-Cerda, N. Tsagarakis, A. Jafari, and D. Caldwell, "Gain scheduling control for a class of variable stiffness actuators based on lever mechanisms," *Robotics, IEEE Transactions on*, vol. 29, no. 3, pp. 791–798, June 2013.

[13] M. W. Spong, "Modeling and control of elastic joint robots," *Transactions of the ASME: Journal of Dynamic Systems, Measurement, and Control*, vol. 109, pp. 310–319, 1987.

[14] S. Nicosia and P. Tomei, "Design of global tracking controllers for flexible-joint robots," *Journal of robotic systems*, vol. 10, no. 6, pp. 835–846, 1993.

[15] A. Loria and R. Ortega, "On tracking control of rigid and flexible joints robots," *Appl. Math. Comput. Sci*, vol. 5, no. 2, pp. 101–113, 1995.

[16] C. Ott, A. Albu-Schäffer, A. Kugi, and G. Hirzinger, "Decoupling based cartesian impedance control of flexible joint robots," in *Proc. IEEE Int. Conf. on Robotics and Automation*, 2003.

[17] J. H. Oh and J. S. Lee, "Control of flexible joint robot system by backstepping design approach," *Intelligent Automation & Soft Computing*, vol. 5, no. 4, pp. 267–278, 1999.

[18] C. Ott, *Cartesian Impedance Control of Redundant and Flexible-Joint Robots*, B. Siciliano and O. Khatib, Eds. Springer, 2008.

[19] J.-J. Slotine and L. Weiping, "Adaptive manipulator control: A case study," *Automatic Control, IEEE Transactions on*, vol. 33, no. 11, pp. 995–1003, 1988.

[20] M. W. Spong, "Adaptive control of flexible joint manipulators," *Systems & Control Letters*, vol. 13, no. 1, pp. 15–21, 1989.

[21] A. De Luca and P. Lucibello, "A general algorithm for dynamic feedback linearization of robots with elastic joints," in *IEEE Int. Conf. on Robotics and Automation*, vol. 1, 1998, pp. 504–510.

[22] G. Palli, C. Melchiorri, and A. De Luca, "On the feedback linearization of robots with variable joint stiffness," in *IEEE Int. Conf. on Robotics and Automation*, 2008, pp. 1753–1759.

[23] A. De Luca and F. Flacco, "Dynamic gravity cancellation in robots with flexible transmissions," in *Decision and Control (CDC), 2010 49th IEEE Conference on*, Dec 2010, pp. 288–295.

[24] M. Keppler, D. Lakatos, C. Ott, and A. Albu-Schäffer, "A passivity-based controller for motion tracking and damping assignment for compliantly actuated robots," in *Decision and Control (CDC), 2016 IEEE 55th Conference on*. IEEE, 2016, pp. 1521–1528.

[25] M. Keppler, D. Lakatos, C. Ott, and A. Albu-Schäffer, "A passivity-based approach for trajectory tracking and link-side damping of compliantly actuated robots," in *2016 IEEE International Conference on Robotics and Automation (ICRA)*. IEEE, 2016, pp. 1079–1086.

[26] A. Albu-Schäffer, C. Ott, and G. Hirzinger, "A unified passivity-based control framework for position, torque and impedance control of flexible joint robots," *The International Journal of Robotics Research*, vol. 26, no. 1, pp. 23–39, 2007. [Online]. Available: http://dx.doi.org/10.1177/0278364907073776

[27] B. Paden and R. Panja, "Globally asymptotically stable ?PD+?controller for robot manipulators," *International Journal of Control*, vol. 47, no. 6, pp. 1697–1712, 1988.

[28] B. Brogliato, R. Ortega, and R. Lozano, "Global tracking controllers for flexible-joint manipulators: A comparative study," *Automatica*, vol. 31, no. 7, pp. 941–956, Jul. 1995.

[29] F. Ghorbel, B. Srinivasan, and M. W. Spong, "On the uniform boundedness of the inertia matrix of serial robot manipulators," *Journal of Robotic Systems*, vol. 15, no. 1, 1998.

[30] J.-J. Slotine and W. Li, *Applied Nonlinear Control*. Prentice Hall, 1991.

[31] A. van der Schaft, *L2-gain and passivity techniques in nonlinear control*. London New York: Springer, 2000.

[32] N. Rouche, P. Habets, and M. Laloy, *Stability Theory by Liapunov's Direct Method*. Springer New York, 1977. [Online]. Available: http://dx.doi.org/10.1007/978-1-4684-9362-7

[33] V. Matrosov, "On the stability of motion," *Journal of Applied Mathematics and Mechanics*, vol. 26, no. 5, pp. 1337–1353, jan 1962. [Online]. Available: http://dx.doi.org/10.1016/0021-8928(62)90010-2

[34] W. Khalil and E. Dombre, *Modeling, Identification and Control of Robots*, 3rd ed. Bristol, PA, USA: Taylor & Francis, Inc., 2002.

[35] C. D. Meyer, *Matrix analysis and applied linear algebra*. Philadelphia, PA: Society for Industrial and Applied Mathematics, 2004.

[36] R. A. Horn and C. R. Johnson, *Matrix Analysis*. Cambridge University Press, 2012.

[37] R. B. Nelson, "Simplified calculation of eigenvector derivatives," *AIAA Journal*, vol. 14, no. 9, pp. 1201–1205, sep 1976.

[38] M. I. Friswell, "Calculation of second and higher order eigenvector derivatives," *Journal of Guidance, Control, and Dynamics*, vol. 18, no. 4, pp. 919–921, jul 1995.

[39] J. K. Merikoski and R. Kumar, "Inequalities for spreads of matrix sums and products." *Applied Mathematics E-Notes*, vol. 4, pp. 150–159, 2004.

Manuel Keppler received his Dipl.-Ing. degree in mechanical engineering with focus on control theory from the Technical University of Vienna, in 2014. Since then, he has been with the German Aerospace Center (DLR), Institute of Robotics and Mechatronics, Wessling, Germany.

His current research interests include modeling and control of nonlinear robotic systems, flexible joint and variable compliance robots, human and robot dynamics design of bio-inspired robots.

Dominic Lakatos received the Dipl.-Ing. degree in mechanical engineering from the University of Applied Sciences Munich, Germany, in 2011. Since 2011 he has been with the Institute of Robotics and Mechatronics, German Aerospace Center, Wessling, Germany. His main research interests include control of nonlinear systems, under-actuated mechanical systems, compliantly actuated systems, human and robotic dynamics, nonlinear oscillations, periodic motions, limit cycles, hybrid dynamical systems, bio-inspired and legged robots.

Christian Ott received the Dipl.-Ing. degree in mechatronics from the Johannes Kepler University (JKU), Linz, Austria, in 2001, and the Dr.- Ing. degree in control engineering from Saarland University, Saarbruecken, Germany, in 2005. From 2001 to 2007, he was with the German Aerospace Center (DLR), Institute of Robotics and Mechatronics, Wessling, Germany. From May 2007 to June 2009, he was a Project Assistant Professor in the Department of Mechano-Informatics, University of Tokyo, Tokyo, Japan. Since then, he has been working at DLR as team leader of the Helmholtz Young Investigators Group for "Dynamic Control of Legged Humanoid Robots". In January 2014, he became head of the Department of Analysis and Control of Advanced Robotic Systems at DLR. His current research interests include nonlinear robot control, flexible joint robots, impedance control, and control of humanoid robots.

Alin Albu-Schäffer Alin Albu-Schäffer received his M.S. in electrical engineering from the Technical University of Timisoara, Romania in 1993 and his Ph.D. in automatic control from the Technical University of Munich in 2002. Since 2012 he is the head of the Institute of Robotics and Mechatronics at the German Aerospace Center (DLR), which he joined in 1995 as a Ph.D. candidate. Moreover, he is a professor at the Technical University of Munich, holding the Chair for "Sensor Based Robotic Systems and Intelligent Assistance Systems" at the Computer Science Department. His personal research interests include robot design, modeling and control, nonlinear control, flexible joint and variable compliance robots, impedance and force control, physical human-robot interaction, bio-inspired robot design and control. He received several awards, including the IEEE King-Sun Fu Best Paper Award of the Transactions on Robotics in 2012; several ICRA and IROS Best Paper Awards as well as the DLR Science Award. He was strongly involved in the development of the DLR light-weight robot and its commercialization through technology transfer to KUKA.